

1101
0101
0101
0011



Improved durability and reduced system complexity of solid oxide fuel cell systems

Olivier Thomann



Improved durability and reduced system complexity of solid oxide fuel cell systems

Olivier Thomann

A doctoral dissertation completed for the degree of Doctor of Science (Technology) to be defended, with the permission of the Aalto University School of Science, at a public examination held in the auditorium K213 at Aalto University on 09 December 2015 at 12 noon.



ISBN 978-951-38-8360-7 (Soft back ed.)
ISBN 978-951-38-8361-4 (URL: <http://www.vttresearch.com/impact/publications>)
VTT Science 112
ISSN-L 2242-119X
ISSN 2242-119X (Print)
ISSN 2242-1203 (Online)
<http://urn.fi/URN:ISBN:978-951-38-8361-4>
Copyright © VTT 2015

JULKAISIJA – UTGIVARE – PUBLISHER

Teknologian tutkimuskeskus VTT Oy
PL 1000 (Tekniikantie 4 A, Espoo)
02044 VTT
Puh. 020 722 111, faksi 020 722 7001

Teknologiska forskningscentralen VTT Ab
PB 1000 (Teknikvägen 4 A, Esbo)
FI-02044 VTT
Tfn +358 20 722 111, telefax +358 20 722 7001

VTT Technical Research Centre of Finland Ltd
P.O. Box 1000 (Tekniikantie 4 A, Espoo)
FI-02044 VTT, Finland
Tel. +358 20 722 111, fax +358 20 722 7001

Cover image: Olivier Thomann, 2012

Juvenes Print, Tampere 2015

Abstract

Solid oxide fuel cells (SOFCs) show great potential for clean and efficient power generation applications. However, their high cost is preventing their market entry. This dissertation focuses on solutions to increase the durability of SOFCs and to reduce the complexity of SOFC systems to drive their cost down.

Chromium poisoning of the cathode is a major issue limiting the durability of SOFCs. This issue is addressed by the development of a protective manganese-cobalt spinel coating for steel interconnects. Coated interconnects were characterised in SOFC relevant conditions and the results showed that the coating fulfilled its main requirements, which are: limitation of chromium transport from the interconnect to the cathode, protection against oxidation of the steel and low and stable area-specific resistance. Evidence was found that another source of chromium is the balance-of-plant (BoP) components upstream of the cathode, an issue which did not receive much attention in the literature. Therefore, a method for measuring chromium evaporation from BoP components was developed and validated on a stainless steel pipe.

SOFC systems based on natural gas commonly include a fuel processing subsystem for fuel steam reforming. The need for an external water source can be eliminated by recycling the steam-rich anode off-gas. Investigations were performed on a pre-reformer with a precious metal catalyst and it was found that adding an anode off-gas recycling loop had no detrimental effect on the activity of the catalyst and carbon formation could be avoided. Additionally, results showed the possibility to generate the hydrogen-containing gas needed to prevent the reoxidation of the anode catalyst during heat-up phase. The results permitted the implementation of an anode off-gas recycling loop in a 10 kW SOFC system. Additionally, the system was heated up without supplying any premixed hydrogen-containing gas, which enables to reduce the complexity of the system.

Finally, the durability of a stack can be improved by seal solutions with limited material interactions. A hybrid seal solution was developed by coating a compressible core with glass layers. The developed seal reduced the leak rate compared to a purely compressible seal. Material interactions were studied with a post-experimental investigation of an SOFC stack. Interactions were limited with the exception of evidence of increased oxidation at the steel/seal/air interface.

Overall, the solution was found to be promising and the obtained results led to the commercialisation of the developed seal solution by Flexitallic Ltd (UK) [1].

Keywords: Fuel cells, SOFC, chromium poisoning, anode off-gas recycling, system heat-up, seal, interconnect, material interactions

Preface

The work presented here has been carried out between 2010 and 2015 at VTT Technical Research Centre of Finland Ltd under the supervision of Professor Peter Lund from Aalto University. I would like to acknowledge financial support from VTT Technical Research Centre of Finland Ltd, the Fuel Cells and Hydrogen Joint Undertaking and Tekes – the Finnish Funding Agency for Innovation.

I am very thankful to my instructors, D. Sc Jari Kiviaho and D. Sc Olli Himanen. You have been of great support during this work and I enjoyed to have the opportunity to perform exciting research in a motivating environment. I am also grateful to Professor Peter Lund for the efficient supervision.

Additionally, I would like to thank D. Sc Markus Rautanen, D. Sc Matias Halinen, D. Sc Mikko Pihlatie, M. Sc Johan Tallgren, D. Sc Andreas Schuler, D. Sc Pekka Simell and M. Sc Risto Parikka. Our collaboration was absolutely essential to the realization of this work.

Additionally, I would like to express my gratitude to Kari Koskela, Juha Järvinen, Jorma Stick and Kai Nurminen. Without your practical, creative and efficient work, this work would have lasted decades. I thank also Kaija Luomanperä and Päivi Jokimies for the gas analysis.

The friends I made in Otaniemi were also of essential support to take my mind off my work when it was needed. Many thanks to Raphael, Florence, Michał, Emile and Melany.

I would like to thank Tuisku for her continuous support during the up and the down of this adventure. Lastly, a big thank for my family, particularly to my parents, Catherine and Matthias and to my grandparents, Leni and Hans, who were great support for my education and during my doctoral studies.

Espoo, August 2015

Olivier Thomann

Academic dissertation

Supervising
professor

Professor Peter Lund
Department of Applied Physics
Aalto University School of Science
Espoo, Finland

Thesis
advisors

Doctor Jari Kiviaho
Fuel Cells and Hydrogen
Smart Industry and Energy Systems
VTT Technical Research Centre of Finland Ltd
Espoo, Finland

Doctor Olli Himanen
Fuel Cells and Hydrogen
Smart Industry and Energy Systems
VTT Technical Research Centre of Finland Ltd
Espoo, Finland

Preliminary
examiners

Professor Anke Hagen
Department of Energy Conversion and Storage
Technical University of Denmark
Roskilde, Denmark

Doctor Magali Reytier
Hydrogen Production Laboratory
French Alternative Energies and Atomic Energy Commission
Grenoble, France

Opponent

Professor Massimo Santarelli
DENERG -Dipartimento Energia
Politecnico di Torino
Torino, Italy

List of publications

This dissertation is based on the following original publications which are referred to in the text as Publications I–VI. The publications are reproduced with kind permission from the publishers.

- I Thomann, O., Pihlatie, M., Rautanen, M., Himanen, O., Lagerbom, J., Mäkinen, M., Varis, T., Suhonen, T. & Kiviaho, J. Development and application of HVOF sprayed spinel protective coating for SOFC interconnects. *Journal of Thermal Spray Technology* 2013, Vol. 22, No. 5, pp. 631–639.
- II Thomann, O., Pihlatie, M., Schuler, J.A., Himanen, O. & Kiviaho, J. Method for measuring chromium evaporation from SOFC balance-of-plant components. *Electrochemical and Solid-State Letters* 2012, Vol. 15, No. 3, pp. B35–B37.
- III Halinen, M., Thomann, O. & Kiviaho, J. Effect of anode off-gas recycling on reforming of natural gas for solid oxide fuel cell systems. *Fuel Cells* 2012, Vol. 12, No. 5, pp. 754–760.
- IV Halinen, M., Thomann, O. & Kiviaho, J. Experimental study of SOFC system heat-up without safety gases. *International Journal of Hydrogen Energy* 2014, Vol. 39, No. 1, pp. 552–561.
- V Rautanen, M., Thomann, O., Himanen, O., Tallgren, J. & Kiviaho, J. Glass coated compressible solid oxide fuel cell seals. *Journal of Power Sources* 2014, Vol. 247, pp. 243–248.
- VI Thomann, O., Rautanen, M., Himanen, O., Tallgren, J. & Kiviaho, J. Post-experimental analysis of a solid oxide fuel cell stack using hybrid seals. *Journal of Power Sources* 2015, Vol. 274, pp. 1009–1015.

Brief description of the content of the publications

Publication I: Protective coatings were applied on interconnect steel material by high velocity oxy-fuel spraying. The coated substrates were tested in long-term exposure tests to assess their high-temperature oxidation behaviour. Conductivity measurement showed that the coated substrate area-specific resistance was stable over time. Additionally, coated interconnect was used in a stack for 6000 hours and post-experimental analysis showed that the coating protected the interconnect from oxidation and exhibited adequate chromium retention.

Publication II: A method for measuring chromium evaporation from balance-of-plant components was developed. The volatile chromium was collected by air sampling through a denuder tube coated with sodium carbonate. Identification of the source of volatile chromium in an SOFC system is crucial for designing strategies to protect the cathode from chromium poisoning.

Publication III: The article focuses on the effect of anode off-gas recycling on the performance of a natural gas pre-reformer. Two scenarios were compared: one in which the pre-reformer was fed with a gas composition corresponding to the one found in an SOFC system equipped with an anode-off gas recirculation loop, and another corresponding to a system operated with steam-reformed natural gas. The reactor performance was higher using the anode-off gas recycling mode and carbon formation was not observed despite the use of conditions in which carbon formation is thermodynamically possible.

Publication IV: A heat-up strategy for an SOFC system was developed to eliminate the need for premixed protective gas cylinders. Firstly, the heat-up strategy was investigated in a pre-reformer test rig. It was found that oxygen inhibits reforming reactions at low temperatures and that this effect can be mitigated by the addition of hydrogen. The heat-up strategy was then successfully tested on a complete 10 kW SOFC system.

Publication V: Hybrid seals were developed by combining layers of compliant glass and Thermiculite 866 material. The hybrid seal combines the advantage of the compressible core material while the interfacial leak paths are blocked by the compliant glass layers. The hybrid seals exhibited very good performance even at compression stress as low as 0.1 MPa.

Publication VI: The article presents the findings of the post-experimental investigation of an SOFC stack. The stack included hybrid seals (compressive materials sandwiched between glass layers) and thin metallic interconnects (0.2 mm). The work included the investigation of the suitability of hybrid seals in an SOFC stack by measuring leak rate, analysing the ability of the seal to compensate for other component manufacturing tolerances, and material interactions between seals and interconnects. Overall, the hybrid seals used in combination with the thin interconnects were found to be effective solutions due to the low leak rate and limited material interactions.

Author's contributions

For Publication I, the author actively took part in results discussions, data analysis and the writing. The author had the principal responsibility for performing the post-experimental analysis of the stack.

For Publication II, the author had the principal responsibility for the design, experiments, data analysis and writing.

For Publication III, the author contributed to results interpretation and participated actively in the writing.

For Publication IV, the author had the principal responsibility for the ex-situ pre-reformer part of the article and participated actively in the writing.

For Publication V, the author contributed to the ex-situ sealing experiments, to results discussions and participated in the writing.

For Publication VI, the author had the principal responsibility for post-experimental investigation, data analysis and writing.

Contents

Abstract	3
Preface.....	5
Academic dissertation.....	6
List of publications.....	7
Author's contributions	9
List of abbreviations and symbols	12
1. Introduction.....	15
1.1 Background and motivation.....	15
1.2 Scope of the dissertation.....	16
2. Solid Oxide Fuel Cells.....	18
2.1 Theory of operation.....	18
2.2 Electrical efficiency of fuel cells	19
2.3 SOFC stack components	21
2.3.1 Electrolyte	21
2.3.2 Anode	21
2.3.3 Cathode	22
2.3.4 Interconnects.....	22
2.3.5 Seals	23
2.4 Fuel processing for SOFC.....	24
2.5 SOFC system layout: an example	25
3. Prevention of chromium poisoning	27
3.1 Protective coating for metallic interconnects (Publication I)	27
3.1.1 Background.....	27
3.1.2 Experimental	28
3.1.3 Results and discussion	29
3.2 Method for measuring chromium evaporation (Publication II).....	34
3.2.1 Background.....	34
3.2.2 Experimental	35
3.2.3 Results and discussion	37

3.2.3.1	Measurement uncertainty	37
3.2.3.2	Effect of temperature on chromium evaporation	37
3.2.3.3	Effect of heat treatment history on chromium evaporation	38
4.	Fuel processing subsystem	40
4.1	Effect of Anode-Off Gas Recycling on the pre-reformer (Publication III)	40
4.1.1	Background.....	40
4.1.2	Experimental	41
4.1.3	Results and discussion	45
4.1.3.1	Risk of carbon formation at thermodynamic equilibrium ...	45
4.1.3.2	Effect of AOGR on the performance of the pre-reformer ..	46
4.1.3.3	Carbon formation during extended holds.....	48
4.2	Generation of anode protective gas with the system pre-reformer (Publication IV)	50
4.2.1	Background.....	50
4.2.2	Experimental	51
4.2.2.1	Ex-situ pre-reformer experiments.....	51
4.2.2.2	System heat-up experiment.....	52
4.2.3	Results and discussion	53
4.2.3.1	Ex-situ pre-reformer experiments.....	53
4.2.3.2	System heat-up experiments	55
5.	Performance and material compatibility of hybrid seals (Publication V and VI)	58
5.1	Background	58
5.2	Experimental	59
5.2.1	Ex-situ leak rate measurement.....	59
5.2.2	Stack testing	61
5.3	Results and discussion	62
6.	Summary and conclusions	70
	References.....	75

Publications I–VI

Abstract

List of abbreviations and symbols

Greek

ε_E	Voltage efficiency
ε_{FC}	Fuel cell efficiency
ε_{sys}	System fuel cell efficiency
ϵ_{th}	Thermodynamic efficiency
η_{act}	activation loss
η_{ohm}	ohmic loss
η_{conc}	concentration loss

Latin

ASR	Area-specific resistance
AOGR	Anode off-gas recycling
BoP	Balance-of-plant
BSE	Back-scattered electron
CTE	Coefficient of thermal expansion
DC	Direct current
E	Fuel cell operating voltage
E°	Reversible voltage at standard condition
E_{Nernst}	Nernst voltage
E_r	reversible voltage
EDS	Energy-dispersive X-ray spectroscopy
F	Faraday constant

G	Gibbs free energy
GHG	Greenhouse gas
GHSV	Gas hourly space velocity
HVOF	High velocity oxy-fuel
H	Enthalpy
I	Current
ICP-MS	Inductively coupled plasma mass spectrometry
LSM	Lanthanum manganite (La,Sr)MnO ₃
LSC	(La,Sr)CoO ₃
LSCF	(La,Sr)(Co,Fe)O ₃
NG	Natural gas
NLPM	Normal litre per minute
NTP	Normal temperature and pressure
P_{AC}	Power supplied by the SOFC stack after conversion to AC
P_{aux}	Power demand of auxiliary devices
p_i	Partial pressure of gas
\dot{Q}_{fuel}	Fuel flow
$\dot{Q}_{H_2}^{cross}$	Hydrogen cross leak
$\dot{Q}_{Air}^{C,in}$	Cathode air inlet flow
R	Universal gas constant
RR	Recycling ratio
SEM	Scanning electron microscopy
SOFC	Solid oxide fuel cell
SR	Steam reforming
T	Temperature
t	Time
THT	Tetrahydrothiophene
V	Volume
$X_{H_2O}^{C,out}$	Steam molar fraction at the cathode outlet

YSZ	Yttria-stabilised zirconia
z	Electrons involved in the electrochemical reaction

1. Introduction

1.1 Background and motivation

The development of a sustainable energy system is one of the global challenges of our times. We need an energy system that fosters economic developments, while having a sustainable footprint on the environment. Emissions of pollution and resource consumption related to the energy sector have to be reduced to acceptable levels. Moreover, the human impact on climate change has been established [2] and significant efforts are being undertaken to curb greenhouse gas (GHG) emissions [3].

Technological developments can contribute to addressing the different challenges of our energy system. Public electricity and heat production accounted for 27% of GHG emissions in Europe in 2012 [4]. Electricity generation is presently dominated by fossil fuel-based generation, with about 50% of European electricity coming from fossil fuels in 2010 [5]). This sector is undergoing deep transformations because of the pressure to reduce the carbon-footprint of electricity, countries phasing out nuclear electricity or reducing its share, and tighter emission regulation on air pollution. Therefore, there is an important commercial potential for technologies that can contribute to increasing the electricity production efficiency and reducing its emissions in terms of pollution and GHG. Fuel cells are perceived to have an important role to play in the power generation in stationary, portable and transport applications due to their high electrical efficiency and very low emissions [6,7].

Fuel cells are electrochemical energy conversion devices that convert chemical energy from fuels directly into electricity and heat. Conversely to thermal power generation, fuel cells do not involve a combustion process. Fuel cells are modular in nature and can be scaled from a small generator (100 W) to an MW-class power plant, which makes them suitable for a wide range of applications. There are different types of fuel cells based on their electrolyte material. The fuel cells operating at the highest temperature are called Solid Oxide Fuel Cells (SOFCs) and operate between 600 and 900 °C. SOFCs have been the subject of intensive research and development because of their specific advantages.

SOFCs can achieve high efficiency even in small power units, with a demonstrated system electrical efficiency of 60% in units as small as 1–2 kW [8]. The

high operating temperature of SOFCs means that they can provide high quality heat for CHP applications. SOFCs have extremely low emissions. Because no combustion is taking place, nitrogen oxide and particulate matter emissions are insignificant. In addition, sulphur oxide emissions are extremely low because sulphur is a poison to SOFCs and is removed from the fuel feedstock before use. SOFCs also emit considerably less noise than combustion engines. The high temperature of operation of SOFCs enables a wide fuel flexibility and they can be designed to operate on hydrocarbon fuels, the infrastructures of which are already well developed. They are therefore a technology of choice for renewable fuels such as biogas, landfill gas, syngas from biomass gasification, biofuels and fuels produced from renewable electricity (power-to-gas route) [9-11] and thus they can additionally contribute to the reduction of GHG emissions and resource depletion.

Despite its advantages, the road to market has proven to be challenging for SOFCs. The main reasons hindering their market entry so far are their high cost, which is partly due to their insufficient durability and high system complexity. However, it should be noted that the market for SOFCs has seen a marked improvement in the last few years with 27 MW of shipped SOFC units worldwide in 2012 [12]. The market is presently driven by the demand for prime power for datacentres in the USA and CHP units in Japan and Europe.

Cost and lifetime targets of SOFCs depend on the specific application. For example, in their multi-annual implementation plan (2008–2013), the Fuel Cell and Hydrogen Joint Undertaking (FCH JU) specifies the SOFC technical targets for large commercial or industrial applications (300 kW – 5 MW) [13]. By 2015, the targets are 20,000 h lifetime at 55% electrical efficiency at a system cost of 4000 € kW⁻¹. By 2020, the targets are a lifetime of 40,000 h at 60% electrical efficiency with a system cost of 2000 € kW⁻¹.

1.2 Scope of the dissertation

The capital cost of an SOFC system is seen as key challenges preventing their market entry; it requires an improvement of their durability and a reduction of the system complexity to drive the overall cost down. The dissertation focuses on a selection of studies that address these challenges at the stack and system level.

One of these challenges is the prevention of cathode performance degradation. Several degradation phenomena can affect the durability of the cathode such as microstructural change, decomposition of the cathode material, chemical reaction with the electrolyte material, spallation of the cathode and chromium poisoning [14]. Despite numerous publications have been published on chromium poisoning, this topic was selected because some questions are still unanswered. It is established that volatile chromium species originating from stainless steel components can deposit on the cathode and degrade their performance over time, leading to insufficient SOFC lifetime. Most effort in research have targeted the development of protective coatings for metallic interconnect, however, the data about the dura-

bility of such coating in stack testing is limited. The publication I presents the results on the development of coating to reduce the transport of chromium from the stainless steel interconnect to the cathode and the coating evaluation in long-term stack test. Additionally, little is published about the transport of chromium from stainless steel balance-of-plant components to the cathode. Therefore, a quantification method was developed to assess the contribution of balance-of-plant components on the chromium intake of the cathode (Publication II).

Another challenge is to simplify the fuel processing subsystem. SOFCs running on natural gas have previously relied on steam reforming to generate a hydrogen-rich gas. The steam necessary for the steam reforming reaction can either be provided from an external source or from the electrochemical reaction in the SOFC itself. An external source of water requires a cleaned water inlet and an evaporator and it significantly increases the complexity of the system. One way of eliminating the cleaned water inlet during operation is to recirculate the steam-rich anode off-gas of the SOFC stack. This solution brings up new challenges for the activity of the reforming catalyst and increases the risk of carbon formation in the pre-reformer. This dissertation includes the results of an experimental study on the effect of anode off-gas recycling on the pre-reformer of an SOFC system (Publication III). Another simplification of the fuel processing subsystem is the elimination of the need for premixed protection gas during the heat-up. Traditionally, the premixed protection gas (4%-vol hydrogen in nitrogen) is used during SOFC heat-up to prevent the nickel of the anode from oxidising. This is a costly solution and increases the system size and maintenance need. Therefore, there is a motivation to generate in-situ the hydrogen-containing protective gas using natural gas and the system pre-reformer. This is addressed by Publication IV. This study presents the results on the generation of hydrogen with steam reforming on precious metal catalyst at temperatures as low as 200 °C. This result was used to develop a heat-up procedure that was used to heat up a 10 kW SOFC system.

The last challenge addressed in this work is the development of durable, low cost, highly conformable seals for an SOFC stack. Seals are needed to prevent mixing of the fuel and the oxidant in the SOFC stacks. Currently, seals are often made of ceramic glass that is brittle and prone to cracking upon thermal cycling. An alternative explored in the dissertation is the use of a composite structure of a mica-type of paper sandwiched between thin layers of glass. Such hybrid seals are not brittle in nature, limit the use of expensive sealing glass and allow larger manufacturing tolerance for SOFC components. The performance of such seals and the material compatibility with other stack components are investigated in Publications V and VI.

2. Solid Oxide Fuel Cells

2.1 Theory of operation

SOFCs produce electricity (and heat) from fuel and air via electrochemical reactions. They are based on cells constituted by gas-tight ionic-conductor ceramic electrolytes in contact with two electrically and ionically conductive electrodes. The operating principle of an SOFC is illustrated in Figure 1. The fuel (typically hydrogen-rich gas) is oxidised at the anode to form water and to release two electrons (Equation 1). The electrons are transported through an external circuit to the cathode. At the cathode, oxygen uptakes the electrons and is reduced to form oxygen ions (Equation 2). The oxygen ions are transported to the anode side through the electrolyte to react with the fuel by the overall reaction expressed in Equation 3.



In order to increase the delivered electrical power, cells are connected in series with electrically conductive interconnects to form a stack.

SOFCs do not require pure hydrogen as a fuel, as opposed to low-temperature fuel cells such as proton-exchange membrane fuel cells. Hydrocarbon fuels such as methane can be reformed inside the stack (as shown in Figure 1) or externally to form a gas mixture rich in hydrogen and carbon monoxide. Methane is reformed according to equation 4 in the anode of the SOFC, which typically includes nickel as a catalyst.



The carbon monoxide reacts further according to the water gas shift reaction (Equation 5) to form hydrogen and carbon monoxide. Therefore, carbon monoxide is not a poison to SOFC, but can be considered as a fuel.

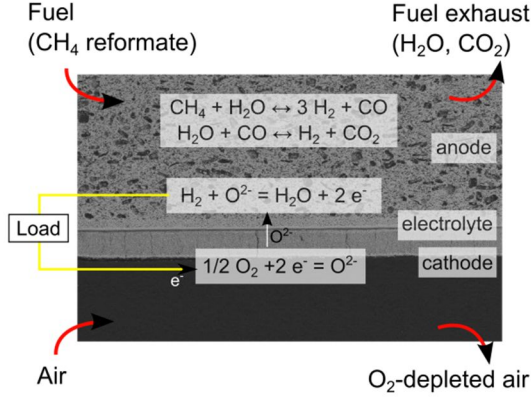


Figure 1. Elementary reaction steps in an SOFC.

2.2 Electrical efficiency of fuel cells

One of the advantages of fuel cells over a thermodynamic cycle engine is that they are not limited by the Carnot efficiency. The maximum achievable work from a chemical reaction is given by the change in Gibbs free energy ΔG . For the same reaction, the maximum amount of heat released (at constant pressure) is given by the change in enthalpy ΔH . Consequently, the maximum thermodynamic efficiency can be defined according to Equation 6.

$$\epsilon_{th} = \frac{\Delta G}{\Delta H} \quad (6)$$

The maximum thermodynamic efficiency therefore depends on the fuel considered. For example, at 700 °C, ϵ_{th} with hydrogen as a fuel is 82%, while for methane, the same value is 99%.

In practice, the maximum thermodynamic efficiency is not achieved because of different irreversibilities.

The theoretical reversible voltage E_r of a fuel cell is given by the available electrical work available, ΔG , divided by the charge transferred in the reaction according to:

$$E_r = \frac{-\Delta G}{zF} \quad (7)$$

where z is the number of electrons taking part in the reaction and F is the Faraday constant.

However, the actual cell voltage is always below the reversible voltage because of different irreversibilities. For example, the gas leakage through the seals or through the electrolyte leads to a voltage drop. Additionally, the electronic conduction of the electrolyte is non-zero and causes a short-circuit of the cell, which also decreases the cell voltage. If the partial pressures of the gas in the fuel cell are known, the Nernst equation can be used to calculate the voltage as a function of temperature and partial pressure of oxygen on the cathode and of the hydrogen and steam on the anode:

$$E_{Nernst} = E^\circ + \frac{RT}{zF} \ln\left(\frac{p_{O_2}^{1/2} p_{H_2}}{p_{H_2O}}\right) \quad (8)$$

where E° is the reversible voltage at standard condition, R is the gas constant, T the temperature and p_i is the partial pressure of the different gases.

In addition, the cell voltage is further decreased when current is drawn from the cell due to activation loss (η_{act}), ohmic loss (η_{ohm}) and concentration loss (η_{conc}). The activation loss corresponds to the overpotential required to overcome the activation energy of the electrochemical reaction. It is a measure of the catalyst effectiveness at a given temperature. The ohmic loss stems from the resistivity of the materials to the current and it is dominated by the ionic resistivity of the electrolyte. The concentration loss is present at high current density when the limitation of mass transport of reactants to the catalysts and the reaction products from the catalyst causes a voltage drop. Therefore, the cell voltage under load is:

$$E = E_{Nernst} - \eta_{act} - \eta_{ohm} - \eta_{conc} \quad (9)$$

One can thus define a voltage efficiency, ε_E , as the quotient of the actual cell voltage over the reversible voltage.

$$\varepsilon_E = \frac{E}{E_r} \quad (10)$$

In addition, not all the fuel is used in the fuel cell, therefore one can define the fuel utilisation, FU , defined as the quotient of the current drawn from the cell and the maximum current that a flow of fuel could deliver:

$$FU = \frac{I}{zF\dot{Q}_{fuel}} \quad (11)$$

where \dot{Q}_{fuel} is the flow of fuel. The fuel utilisation is typically between 70 and 90% in an SOFC.

The fuel cell efficiency, ε_{FC} , is obtained by multiplying the efficiency components (Equations 6 and 10) and the fuel utilisation (Equation 11):

$$\varepsilon_{FC} = \varepsilon_{th} \varepsilon_E FU = \frac{E I}{-\Delta H n_{fuel}} \quad (12)$$

which is the electric power produced in the cell divided by the chemical power of the fuel flow.

In fuel cell systems, auxiliary devices, such as the blowers, cause parasitic losses. In addition, the current cable and the direct to alternating current convertor cause additional losses. If we assume that the auxiliary devices use grid electricity, the fuel cell system efficiency, ε_{sys} , can be expressed as:

$$\varepsilon_{sys} = \frac{P_{AC}}{-\Delta H n_{fuel} + P_{aux}} \quad (13)$$

where P_{aux} is the power demand of auxiliary devices and P_{AC} corresponds to the alternating current power supplied by the fuel cell to the grid after conversion to alternating current.

Presently, the highest SOFC system efficiency reported in the literature is 60% from natural gas (lower heating value) to net export of alternating current electricity to the grid [8].

2.3 SOFC stack components

2.3.1 Electrolyte

The electrolyte needs to transport oxygen ions from the cathode to the anode, to be electronically insulating and to be dense to avoid the mixing of the fuel and the air atmosphere. It also needs to be stable in reducing and oxidising atmospheres and chemically and physically compatible with the electrode materials. The materials of choice are dense ceramic and the most commonly used is yttria-stabilised zirconia (YSZ) [15].

2.3.2 Anode

The anode needs to be catalytically active towards hydrogen oxidation, electrically conductive to direct the electrons to the interconnect, ionically conductive and its material should be stable in reducing conditions. Commonly, nickel is used in combination with YSZ in a porous cermet (a composite material of metal and ceramic). Nickel offers sufficient catalytic activity and is a good electrical conductor. In addition, it is also catalytically active towards steam reforming of methane, which is a significant advantage because it allows the use of methane as a fuel as explained in more detail in Section 2.4. The YSZ phase allows the transport of

oxygen ions towards the electrochemically active anode sites, at the triple-phase boundary between the nickel, the YSZ and the hydrogen-rich atmosphere [15].

2.3.3 Cathode

The requirements for the cathode are to be active for oxygen reduction, transport of the oxygen ions to the electrolyte and distribution of electric current associated with the cathode reaction. Perovskite materials such as doped-lanthanum manganite (La,Sr)MnO₃ (LSM) have been extensively used as cathode material. However, LSM is a largely electronic conductor, which restricts the reaction to the triple-phase boundary with the YSZ material. In order to increase the cathode active site, mixed ionic electronic conductor perovskites are also used as a cathode material, such as (La,Sr)CoO₃ (LSC) [16] and (La,Sr)(Co,Fe)O₃ (LSCF) [17].

A major issue with SOFC cathodes is the so-called chromium poisoning. Chromium evaporates from metallic interconnect and other steel balance-of-plant components and is transported to the cathode, where it deposits and degrades the cathode properties [18,19].

2.3.4 Interconnects

Interconnects have several functions in an SOFC stack. They collect electrons at electrodes and transport them to the neighbouring cells. In addition, they separate the fuel-rich atmosphere of the anode and the oxygen-rich atmosphere of the cathode. The simultaneous exposure to reducing and oxidising atmospheres at temperatures between 600 and 800 °C sets the high-temperature corrosion resistance requirement very high. Lastly the interconnects ensure the homogenous distribution of fuel and oxidants to the entire electrode surface [20-22].

The requirements of the interconnect materials are therefore:

- i) High electrical conductivity
- ii) High corrosion resistance
- iii) Coefficient of thermal expansion matching with those of the other components of the cell and stack
- iv) Suitable mechanical properties at elevated temperature
- v) Low cost materials and manufacturing method.

For SOFCs operating at temperatures as high as 1000 °C, ceramic interconnects, such as doped-lanthanum chromite, are needed due to the challenging conditions [20]. Thanks to progress in SOFC manufacturing, there has been a general trend towards lowering the operating temperature of SOFCs to 600–800 °C, which allows the use of stainless steel as interconnect materials. Compared to ceramic interconnect material, stainless steels are generally more conductive, cheaper and easier to manufacture and shape. The high electrical conductivity requirement eliminates the alumina-forming stainless steels. The need for coefficient of thermal expansion (CTE) matching with the YSZ (about $10 \times 10^{-6} \text{ }^{\circ}\text{C}^{-1}$ from 25 to 1000 °C)

eliminates the austenitic stainless steels due to their higher CTE. Therefore, most of the research has focused on using ferritic stainless steels for interconnect applications [23]. Several commercial alloys were developed for this specific purpose, such as Crofer 22 APU (ThyssenKrupp VDM), E-Brite (Allegheny Ludlum), ZMG (Hitachi), or Sandvik Sanergy HT (Sandvik Materials Technology). They contain between 20–25% of chromium to meet the CTE and corrosion resistance requirements [24]. In order to further decrease the interconnect material cost, general purpose stainless steel alloys such as AISI 441 are being investigated in combination with corrosion protective coating [25-29].

2.3.5 Seals

The development of effective sealing solutions that address all the seal requirements is essential for improving the durability of SOFC stacks and reducing their cost [30,31]. Seals need to exhibit a low leak rate to decrease fuel loss (fuel leaking to air side and vice versa). Moreover, if the leak is localised, the air leaking to the anode side can cause local reoxidation of the nickel of the anode and can cause the cell to crack. Another issue with localised leakage is the formation of a hot spot, a local increase in the temperature due to the exothermal reaction of fuel and oxidant, which increases the degradation rate of the stack [32]. They need to withstand simultaneous exposure to the air side and to the fuel side at temperatures between 600 to 900 °C. Additionally, their performance should not be affected by hundreds to thousands of thermal cycles for stationary and mobile applications respectively. Moreover, they need to be chemically compatible with the adjacent components like the interconnects and cell materials over the lifetime of the SOFC stack. The seal material should be electrically insulating to avoid short-circuiting. Lastly, the seals should also be inexpensive, easy to assemble and compensate for the manufacturing tolerances of the other stack components.

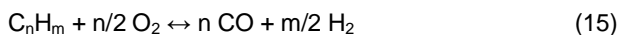
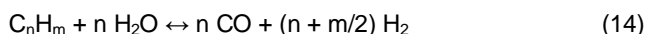
Currently, glass ceramic seals are widely used in SOFC stacks. Their wet adjacent surfaces form a very gas-tight structure (e.g. $0.01 \text{ ml (min m)}^{-1}$ [33]) with few interfacial leakages. However, their main drawback is that the glasses are fragile and withstand tensile stress poorly, which makes them susceptible to failure when thermo-mechanical stresses are present, especially during thermal cycling. Additionally, the properties of glass or glass-ceramics (such as the coefficient of thermal expansion (CTE)), viscosity and porosity change over time, and these changes can create additional thermo-mechanical stresses during long-term operation and increase the risk of seal failure [31,34].

Compressive seals composed of mica-type paper have been investigated as an alternative [32,35,36]. Because compressive seal material exhibits some deformability and the seals are not rigidly bonded to the adjacent surface, they are more resistant to thermo-mechanical stresses. However, their leak rates are usually higher and are dominated by the interfacial leak paths, especially at low compression stresses [37,38].

2.4 Fuel processing for SOFC

SOFCs have a significant advantage over low-temperature fuel cells in the field of fuel flexibility. Because they operate at high temperatures, i.e. 600–900 °C, methane can be reformed on the nickel cermet anode, carbon monoxide does not poison the anode catalyst, and recoverable heat is available for steam reforming reaction [39-41]. Therefore, SOFCs can use a wide range of hydrocarbon fuels from renewable or fossil sources with a relatively simple fuel processing subsystem. They have been operated on biogas [42], natural gas [43], liquefied petroleum gas reformat [44], propane [45], methanol [46] and diesel reformat [47].

Hydrocarbon fuels are typically processed by steam reforming (SR) according to equation 14, by catalytic partial oxidation (Equation 15) or by oxidative-steam reforming, which uses a mixture of air and steam as a reforming agent. Steam reforming is a very endothermic reaction with a change of enthalpy ΔH°_r of +206 kJ mol⁻¹ for methane, while catalytic partial oxidation is exothermic with $\Delta H^\circ_r = -38$ kJ mol⁻¹ for methane [48].



Natural gas is currently widely used as a fuel for SOFCs due to the availability of its infrastructure and low requirements for fuel processing. Its exact composition depends on its source but the main compounds are methane and light hydrocarbon like ethane and propane. A typical natural gas composition from the grids of the United States, Australia, Denmark and Finland are listed in Table 1.

Table 1. Natural gas composition from various national grids.

Natural gas grid from	Main components				
	CH ₄	C ₂ H ₆	C ₃ H ₈	CO ₂	N ₂
USA [49]	87–97	1.5–7	0.1–1.5	0.1–1	0.2–5.5
Australia [8]	91.0	5.0	0.5	2.4	1.0
Danmark [50]	89.1	6.0	2.4	1.0	0.3
Finland [51]	97.9	0.9	0.3	0.0	0.8

Typically, the natural gas is partially reformed before the stack in a pre-reformer. On the one hand, it is beneficial to maintain some internal reforming inside the stack because the endothermic steam reforming reaction cools down the stack, which reduces the need for stack cooling with excess cathode air and the parasitic loss associated with the air blower. On the other hand, a high degree of internal reforming causes a large temperature gradient and thermal stress at the anode

inlet and is detrimental to the durability of the stack [52]. Additionally, there is a risk of carbon formation at the anode at high degrees of internal reforming and this risk increases with higher hydrocarbon fraction [53,54]. In order to decrease the degree of internal reforming, a natural gas-fuelled SOFC system typically includes a pre-reformer upstream of the stack. In the pre-reformer, the fuel is converted to syngas (methane, carbon monoxide and dioxide, hydrogen and steam). The degree of conversion depends on the steam-to-carbon ratio and the pre-reformer temperature.

2.5 SOFC system layout: an example

The scope of this section is not to provide an exhaustive introduction to SOFC systems, but rather to present a specific layout. This specific layout is relevant to the present work because the experiments of Publications III and IV were designed to produce results applicable to this system. The SOFC system is illustrated in Figure 2 and consists of the stack module and the BoP components module. A detailed description of this system and its performance can be found in [43]. The system uses an anode off-gas recycling (AOGR) loop, which enables operation without an external water supply when sufficient steam is produced in the stack. The natural gas is fed to the system and mixed with the recycled anode exhaust gas before being heated up in the fuel heat exchanger. The fuel is then partially reformed in the pre-reformer and fed to the stack. The stack fuel outlet gas is used to heat up the inlet fuel and then a fraction of the fuel is recycled by the AOGR blower. An important parameter is then the recycling ratio (RR), which corresponds to the fraction of the flow of recycled gas over the total flow of anode off-gas. The rest of the fuel exhaust gas is fed to a catalytic burner, where the unreacted fuel fraction is burned with the exhaust air. The heat produced in the catalytic burner is used to heat up the inlet air. The inlet air is fed to the system by an air blower and heated up in the air heat exchanger before being fed to the stack. Additionally, two by-pass valves are used to control the temperature of the stack and the burner. In addition, two electric heaters are used during start-up, one before the stack inlet inside the stack module and another one before the AOGR blower. The system is designed to be thermally self-sustained during operation.

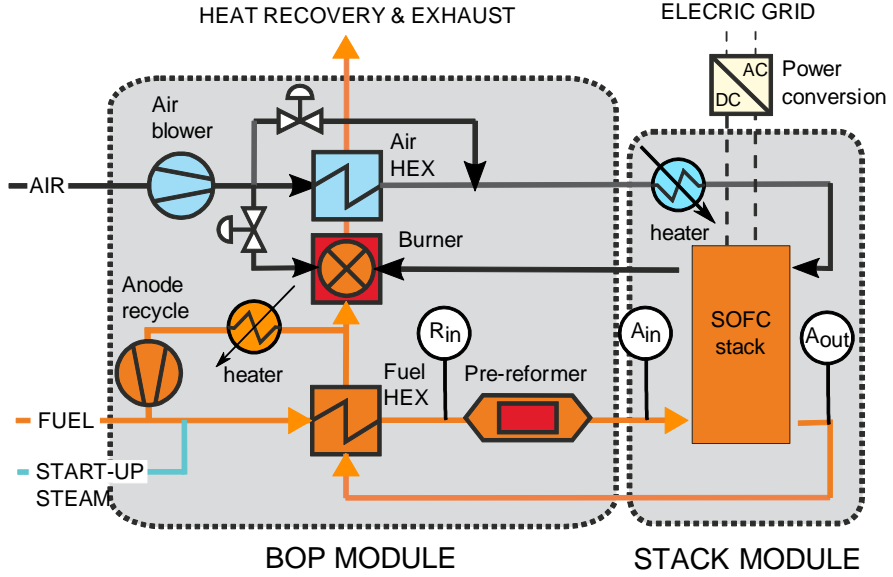


Figure 2. VTT 10 kW demo unit layout with fuel system gas sampling locations. Reproduced and adapted from Ref. [43]. Copyright 2011, The Electrochemical Society.

As mentioned, not all the fuel is used in the stack and this is described by the stack fuel utilisation parameter (FU_{stack}) (Equation 11). As discussed in Section 2.2, it is beneficial to have high fuel utilisation for electrical efficiency. However, there is an optimal value for the stack fuel utilisation because concentration voltage loss becomes important at high fuel utilisation. Moreover, if all the fuel is used in the stack, the nickel of the anode starts to oxidise from the stack outlet, which is highly detrimental to the cell integrity. In a system equipped with an AOGF loop, part of the unused fuel is recycled, which means that the system fuel utilisation (FU_{sys}) becomes higher than the stack utilisation. System fuel utilisation can be calculated from the stack fuel utilisation with Equation 16 [55].

$$FU_{sys} = \frac{FU_{stack}}{1 - RR + RR \cdot FU_{stack}} \quad (16)$$

For example, the VTT 10 kW demo unit operates at about 80% system fuel utilisation, while the stack fuel utilisation is kept at about 60% in nominal conditions.

3. Prevention of chromium poisoning

3.1 Protective coating for metallic interconnects (Publication I)

3.1.1 Background

Ferritic stainless steels are widely used as interconnect materials because they offer an advantageous balance between the fulfilment of their different requirements such as good electrical conductivity, matching of CTE with cell materials and the low cost associated with the material and manufacturing methods [56]. However, the thermally grown oxide layer is mainly composed of chromium oxide and is a source of volatile chromium species, which have been found to deposit on the cathode and cause the so-called chromium poisoning. Chromium poisoning decreases the performance of the cathode over time, which reduce the durability of SOFC [19,57,57-62]. Some ferritic stainless steel alloys were specifically designed for SOFC operation such as Crofer 22 APU (ThyssenKrupp VDM), E-Brite (Allegheny Ludlum, or ZMG (Hitachi) and they form an outer chromium-manganese spinel layer with a lower area-specific resistance (ASR) and a lower chromium evaporation rate (up to 75% reduction of evaporation rate) [58]. However, the reduction of chromium evaporation brought about by optimised steel composition is seen as insufficient and a protective coating is necessary to further reduce the chromium evaporation rate and thus improve the durability of SOFCs [23].

In order to reduce chromium evaporation and oxidation of stainless steel, protective coatings need to have no porosity or closed porosity and low diffusivity of oxygen and chromium through the coating. Moreover, the addition of a coating should not decrease the performance of the SOFC and therefore a coating needs to have a low and stable ASR and good chemical, physical and structural compatibility with the adjacent components.

A wide range of protective coatings have been reported in the literature [23] and among them $(\text{Mn}, \text{Co})_3\text{O}_4$ has received attention for its good performance [63-66]. Numerous methods have been used to deposit such coatings like slurry spraying [67,68], radio-frequency sputtering [68], magnetron sputtering [69,70], plasma spraying [71], atomic layer deposition [72], pulsed laser deposition [73], electro-deposition [74], and filtered arc [75]. In addition, $\text{MnCO}_{2-x}\text{Fe}_x\text{O}_4$ spinel coating has been tested for its better electrical conductivity [65,66].

The goal of the work reported in Publication I was to assess the performance of MnCo_2O_4 and $\text{MnCo}_{1.8}\text{Fe}_{0.2}\text{O}_4$ spinel coatings on Crofer 22 APU steel by high velocity oxy-fuel (HVOF) spraying. Thermal spraying was chosen because it produces coatings that are already very dense and additional sintering is not necessary because the coating is formed by molten or semi-molten droplets. Among thermal spraying method, HVOF spraying was selected because it produces coating with a high tensile bond strength [76]. For this purpose, high-temperature oxidation behaviour and ASR of the coated steel samples were investigated. Additionally, a post-experimental analysis was performed on a single-cell stack using a coated interconnect that was operated for 6000 h. The post-experimental analysis focussed on the evaluation of the coating microstructure, the oxidation of the interconnect, and the transport of chromium. To the authors' knowledge, $(\text{Mn},\text{Co})_3\text{O}_4$ and $\text{MnCo}_{2-x}\text{Fe}_x\text{O}_4$ spinel coatings deposited by HVOF spraying for SOFC interconnects have not been previously reported in scientific journals.

3.1.2 Experimental

Coated Crofer 22 APU test coupons were prepared to evaluate their high temperature oxidation behaviour and to measure their ASR over time. Commercial Crofer 22 APU steel (ThyssenKrupp VDM) with a thickness of 0.2 mm was used as a substrate for test coupons. The coupons were coated by HVOF spraying with a Praxair HV2000 spray gun fitted with a combustion chamber. Nitrogen was used as powder carrier, hydrogen as fuel and air as oxidant.

The high-temperature behaviour was investigated in exposure tests with 10 x 10–15 x 0.2 mm coated coupons. The samples were coated on both sides and only the edges were uncoated. The test was conducted in humidified air (3% vol. steam) for 1000 h at 700 °C. Cross-sections were prepared from the sample for scanning electron microscopy (SEM) observation.

The ASR of the coated interconnect needs to be low and stable over time. For this reason, the ASR was measured for 1000 h at 700 °C in a test arrangement illustrated in Figure 3. The test samples consisted of two coatings ($\text{MnCo}_{1.8}\text{Fe}_{0.2}\text{O}_4$ and MnCo_2O_4) deposited on two 26 x 26 x 0.2 mm steel coupons separated by a ceramic spacer mimicking a cathode. In addition, an uncoated steel plate was tested as a reference. Green $\text{La}_{0.85}\text{Sr}_{0.15}\text{Mn}_{1.1}\text{O}_3$ (LSM) spacers (20 x 20 x 1 mm, IRD Fuel Cells A/S, Denmark) were used as separation material in order to serve as a contact surface with a material similar to an SOFC cathode. Therefore, the investigated contact resistance interface was coated steel against LSM. Several samples were stacked up and a vertical load of 20 N was applied to the samples. Steel plates of 1 mm thickness were used as separator disks between each substrate-coating system. All samples were connected in a single direct current (DC) loop with a current density of 0.2 A cm⁻². The samples were slowly heated up in flowing air to burn off the binder from the green LSM spacers, until 850 °C. The samples were held at 850 °C for 12 hours to sinter the LSM spacer. The steady-state measurements were conducted at 700 °C in dry air. The ASR reported corresponds to half of the ASR measured for one substrate-coating system. The use

of an LSM spacer in the system mimics the contact interface between the coated interconnect and the cathode. However, in a real stack, the sintering of the cathode is performed before stack assembly, whereas the LSM spacers were sintered with the coated substrates in the ASR set-up.

The $\text{MnCo}_{1.8}\text{Fe}_{0.2}\text{O}_4$ coating was tested in a single-cell stack for 6000 h at 700 °C. The interconnects were made of Crofer 22 APU plate with a thickness of 1 mm and the gas channels were etched into the plates. The protective coating was sprayed on the cathode interconnect and was about 20 μm in thickness in its as-sprayed condition. The coated interconnect was not heat-treated prior to use and no contact coating was used. An anode-supported cell with an $(\text{La}, \text{Sr})(\text{Co}, \text{Fe})\text{O}_3$ (LSCF) cathode was used. Dry hydrogen and dry air were used as fuel and oxidant. The current density was 0.3 A cm^{-2} .

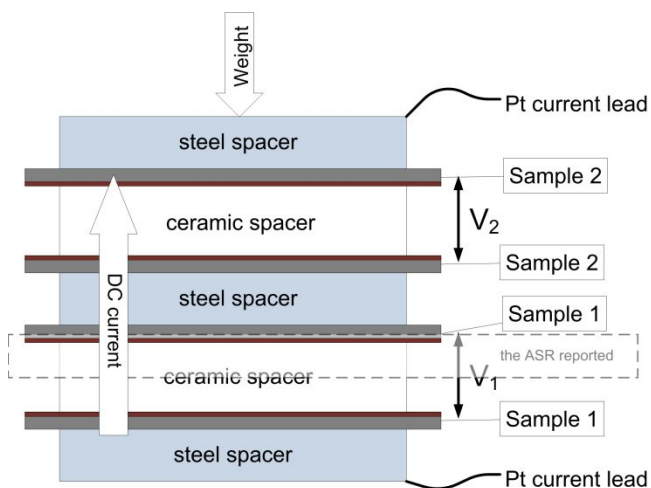


Figure 3. The ASR measurement arrangement for coated Crofer 22 APU coupons with LSM spacers. The protective coatings were applied on the Crofer 22 APU steel surfaces facing the ceramic spacers.

3.1.3 Results and discussion

A typical microstructure of an MnCo_2O_4 as-sprayed coating made by HVOF is presented in Figure 4. The coating exhibits an adequate density. Some alumina particles are visible at the steel-coating interface from the steel grit blasting procedure. The coatings were subjected to exposure to air at 700 °C for 1000 h. Figure 5 illustrates a cross-section of an exposed steel coupon with an $\text{MnCo}_{1.8}\text{Fe}_{0.2}\text{O}_4$ coating of about 17 μm in thickness. The microstructure of the coating is shown in Figure 5 (a) and (b) and an elemental profile from an energy-dispersive X-ray spectroscopy (EDS) line scan is presented in Figure 5 (c). The thermally grown chromium oxide layer between the steel and the coating is about 0.5 μm in thickness. During high-temperature exposure, the coating sintered and lost its lamellar

structure. Some closed porosity remains visible after 1000 h of exposure with a decreasing porosity towards the surface. The elemental profile shows that there is little or no chromium gradient in the coating, which suggests that the diffusion of chromium is effectively hindered. As a reference, a non-coated Crofer 22 APU sample exposed to the same condition exhibited a thermally grown chromium oxide layer of about 2.5 μm in thickness, which is five times higher than the coated sample. Therefore, the coating solution effectively reduces the oxidation of the steel interconnect.

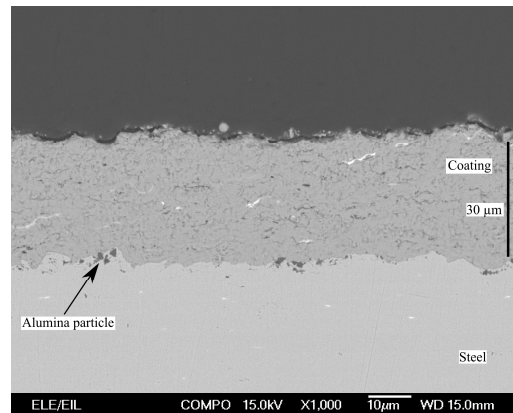


Figure 4. A SEM-BSE image of an as-sprayed HVOF MnCo₂O₄ coating on a Crofer 22 APU substrate.

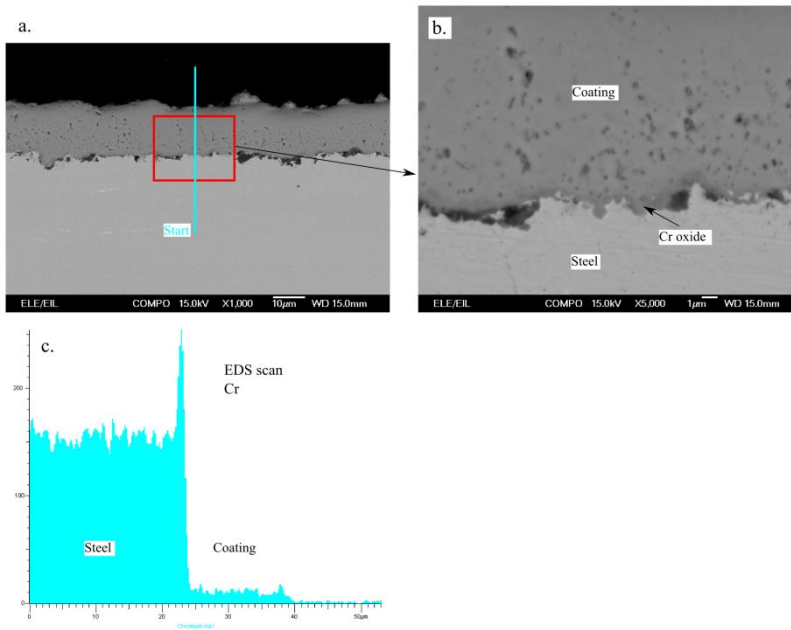


Figure 5 (a and b). SEM-BSE images of an HVOF $\text{MnCo}_{1.8}\text{Fe}_{0.2}\text{O}_4$ coating on a Crofer 22 APU substrate exposed to air at 700 °C for 1000 h at different magnification. c. Measured chromium EDS profile.

The ASR measurements versus time for coated and uncoated stainless steel coupons are presented in Figure 6. The ASR values included the contribution of different components, which are the steel substrate, the chromium oxide scale developing on the steel surface, the protective coating, the contact resistance of the interface between the coating and the ceramic cathode material, and the resistance of the ceramic cathode material (i.e. 500 μm of LSM). A few step changes in the ASR took place at 220 and 720 h and are associated with either structural instability or small unintentional changes in the test temperature (10 °C) due to a power failure. The ASRs of the $\text{MnCo}_{1.8}\text{Fe}_{0.2}\text{O}_4$ (17 μm thick) and the MnCo_2O_4 (20-28 μm thick) coatings were initially between 20 and 30 $\text{m}\Omega\text{cm}^2$ and stabilised at about 20 $\text{m}\Omega\text{cm}^2$ after a few hundred hours. The ASRs then remained stable until the end of the test after 1000 h. These results suggest that the electrical properties of the coated stainless steel samples do not degrade when exposed to air at high temperatures. It is difficult to compare ASR results between different studies because the experimental parameters, such as measurement temperature, test duration, gas atmosphere, contact material and the spacer used vary widely throughout the literature. However, the ASR results reported here are in

line with results obtained for MnCo_2O_4 spinel coatings deposited by a slurry-coating technique [77] or using a similar test arrangement including cathode material spacers [68,78].

The ASR of the uncoated Crofer 22 APU in contact with the LSM spacer was initially about $100 \text{ m}\Omega\text{cm}^2$ and decreased during the tested period to reach $45 \text{ m}\Omega\text{cm}^2$ after 1000 h. The observed decrease in ASR over time is attributed to the formation of a conductive $(\text{Cr}, \text{Mn})_3\text{O}_4$ spinel layer on top of the oxide layer, which improves the electrical contact between steel and LSM. This behaviour was previously observed by Yang et al. [68,79]. In principle, the observed decrease in ASR could also be attributed to possible sintering of the green LSM spacer and consequent increasing of its bulk conductivity, however this initial improvement was not observed for the coated samples that were also using green LSM spacers. The ASR of both coated samples was initially smaller than the uncoated Crofer 22 APU, which is counterintuitive because the coating is expected to have some resistance. Therefore, it is believed that the initial difference originates from a lower contact resistance of the coated samples.

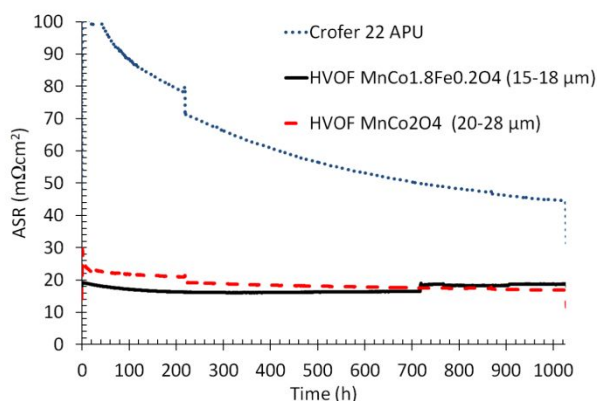


Figure 6. Measured ASR in a 4-point DC measurement of Crofer 22 APU coupons, coated and uncoated, all in contact with an LSM spacer. The coatings are $\text{MnCo}_{1.8}\text{Fe}_{0.2}\text{O}_4$ and MnCo_2O_4 .

Finally, a post-experimental analysis was performed on a single-cell stack that used a coated interconnect. The aim of the post-experimental analysis was to assess the performance of the coating in terms of interconnect oxidation and retention of chromium. Four back-scattered electron (BSE) SEM cross-sections of the single-cell stack are illustrated in Figure 7. Figure 7 (a) presents a low-magnification view of the cathode side where the air channel and the contact location between the cathode and the coated interconnect are visible. The coating

covers the interconnect completely, including geometrically challenging features like the edges of the interconnect ribs.

Figure 7 (b) shows the contact location between the cathode and the interconnect coated with $\text{MnCo}_{1.8}\text{Fe}_{0.2}\text{O}_4$. The chromium oxide scale is about $1\text{ }\mu\text{m}$ in thickness after 6000 h at $700\text{ }^\circ\text{C}$ in air. Figure 7 (c) shows the coated interconnect at an air channel location. The chromium oxide scale below the coating is also about $1\text{ }\mu\text{m}$ in thickness. These results can be compared with the exposure tests presented above where the chromium oxide layer of the coated steel was about $0.5\text{ }\mu\text{m}$ in thickness and the oxide layer of the uncoated steel was about $2.5\text{--}3\text{ }\mu\text{m}$ after 1000 h in air at $700\text{ }^\circ\text{C}$. Therefore, the coating solution appears to effectively reduce the oxidation of the interconnect in a long-term test in an SOFC environment. The elemental composition of the coatings at both locations was analysed by EDS but no chromium could be detected (detection limit is about 0.3%-at), which indicates that the diffusion of chromium is effectively hindered by the coating. The chromium content of the cathode was also investigated and no chromium could be detected in the cathode at the interconnect contact location (Figure 7 (b)). Figure 7 (d) illustrates the cathode at an air channel location and an EDS chromium concentration profile across the cathode. The EDS analysis reveals that chromium was present in the cathode at this air channel location. Chromium distribution is inhomogeneous and peaks at 2.1%-at. The chromium source for this contamination can either be the stainless steel interconnect, coming through the protective coating, or the uncoated Crofer 22 APU air manifold and Inconel 600 air inlet pipe upstream of the stack. However, chromium contamination was only found at the air channel location (Figure 7 (d)) and not at the contact location with the interconnect (Figure 7 (b)), which supports the hypothesis that the chromium has originated from the uncoated air manifold and inlet pipe. Additionally, the EDS analysis showed that no chromium could be detected in the coating, suggesting that negligible chromium diffusion appears to take place across the coating. Stainless steel components and manifold upstream of the cells have been previously identified as chromium contamination sources [80] and the work presented in Publication II also shows that BoP components can be a significant source of volatile chromium [81].

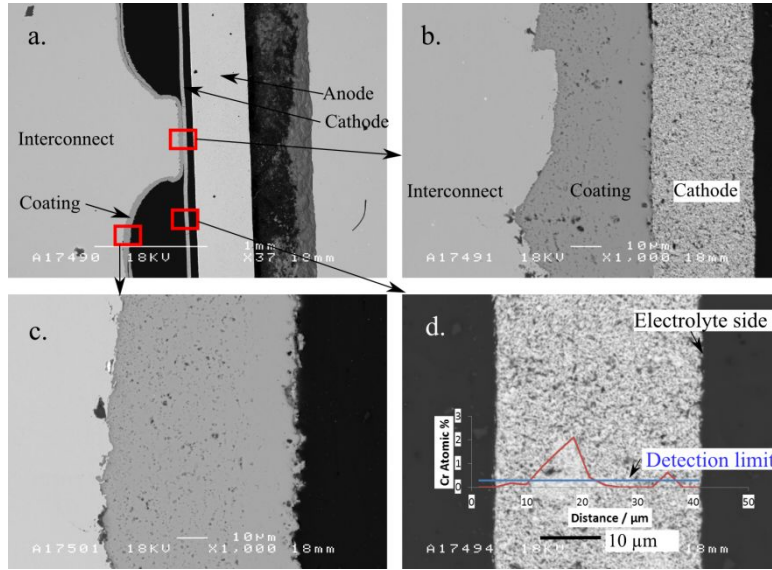


Figure 7. SEM-BSE cross-section from the single-cell stack at different locations. (a) Low-magnification image of the air side of the single-cell stack. The interconnect coating composition is $\text{MnCo}_{1.8}\text{Fe}_{0.2}\text{O}_4$. (b) The contact area between coated interconnect and cathode. (c) Surface of the interconnect at an air channel location. (d) Cathode with an EDS chromium profile.

3.2 Method for measuring chromium evaporation (Publication II)

3.2.1 Background

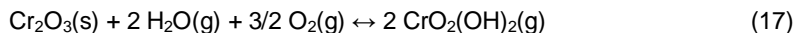
As discussed in Section 3.1, chromium poisoning of cathode is seen as one of the major issues with respect to the durability of SOFCs. A large amount of literature has been dedicated to the development of solutions to reduce the transport of chromium from stainless steel interconnect materials to the cathode. Section 3.1 presented such a solution in the form of a protective coating applied by HVOF spraying. However, metallic interconnects are not the only possible source of chromium in an SOFC system. Commonly, the high-temperature BoP components, such as piping and heat exchangers, are made of austenitic stainless steels for their better mechanical and corrosion properties and are thus also a potential source of volatile chromium species [58]. The chromium volatile species can then be transported from the BoP component upstream of the stack to deposit on the cathode as proposed in [82,83]. Due to the relative complex geometry of BoP

components, most of the coating techniques developed for interconnects are not applicable to BoP components. An assessment of chromium evaporation rates from BoP components is therefore seen as a prerequisite for the development of solutions to reduce this effect and the evaluation of improvements brought about by such solutions. These include material selection [84], surface treatment such as aluminising [85,86], coatings or chromium trapping [87]. Publication II aims to contribute to this challenge by presenting a dedicated measurement technique.

Several methods to quantify chromium evaporation have been reported in the literature and were reviewed in [88]. They all rely on the evaluation of small metal coupons [58,89,90]. These methods are well adapted to comparing different samples. However, it is difficult to calculate from their results the actual amount of chromium coming from a real complex-shaped component (uneven temperature and flow profile and large surface area), as the evaporation rate depends on several factors like the flow rate, flow regime and local temperature. This work focuses on the development of a method for measuring chromium evaporation directly from the hot gas stream of a BoP component. The chromium collection is carried out by using a coated denuder tube, a technique previously used by Froitzheim et al. [89].

3.2.2 Experimental

The schematic drawing of the experimental set-up is illustrated in Figure 8. An austenitic stainless steel pipe was evaluated as a simple BoP component. However, the method could be used on a more complex component, e.g. a heat exchanger. The 1.2 m long pipe was of grade 253MA (Sandvik) and its composition is given in Table 2. It was exposed to a high temperature in a furnace. Humidified air (1.8 vol-% humidity) was fed into the pipe at a rate of $10 \text{ l}_N \text{ min}^{-1}$. A quartz denuder tube (inner diameter 5.2 mm and length 500 mm) was inserted into the steel pipe near its end. A fraction of the flow (from 15 to 35% of the main flow) was sampled through this denuder tube by a diaphragm pump and a rotameter. The inner wall of the denuder tube was dip-coated with sodium carbonate from a surfactant-containing solution. In the presence of humidity, the dominant species in air is chromium oxyhydroxide which is formed according to equation (17) [91].



The chromium oxyhydroxide reacts with the sodium carbonate coating according to the equation (18). According to HSC [92], the equilibrium constant of this reaction is above 10^{10} from room temperature to 800 °C.



Each measurement lasted 24 hours, after which the coated denuder tube was replaced without cooling down the furnace, which is very time-efficient to perform

repeated experiments. The chromium-containing coating was dissolved in 10% nitric acid, diluted to obtain a suitable chromium concentration for inductively coupled plasma mass spectrometry (ICP-MS, Thermo Scientific ELEMENT 2). The effect of temperature of the stainless steel pipe on the chromium evaporation rate was investigated by triplicated measurements that were carried out at 650, 700 and 750 °C.

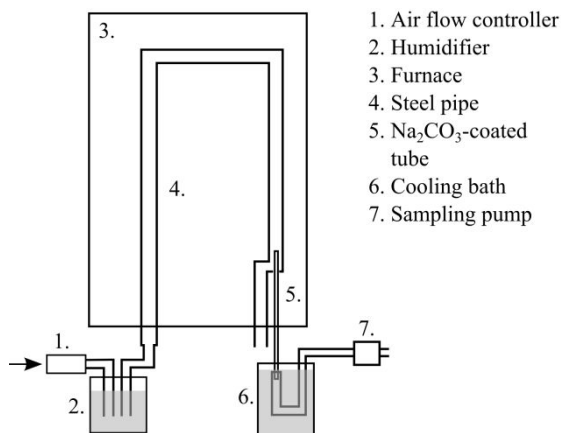


Figure 8. Schematic drawing of the experimental set-up.

The effect of the heat treatment history of the stainless steel pipe was investigated by measuring the chromium evaporation rate at 750 °C before and after a heat treatment at 800 °C for 100 hours. SEM and EDS were used to investigate the correlation between the change of evaporation rates and microstructure of stainless steel oxide layers.

Table 2. Nominal chemical composition of 253MA in %-weight [93].

C	Si	Mn	P	S	Cr	Ni	N	Ce
0.08	1.6	≤0.8	≤0.04	≤0.03	21	11	0.17	0.05

3.2.3 Results and discussion

3.2.3.1 Measurement uncertainty

It was verified that the coated denuder tube was sufficiently long for chromium collection by assessing that most of the chromium collected ($70.7 \pm 17.2\%$) reacted in the first third of the tube. Actually only $7.3 \pm 1.8\%$ of the total amount of chromium collected reacted in the last third of the tube. Sodium carbonate coated denuder tube can reach very high collection efficiency, for example, Froitzheim et al. used a similar set-up to measure chromium evaporation from steel coupons and they demonstrated a collection efficiency of 95% [89].

Measurement error on the chromium concentration in air was calculated to be 6% based on the errors of the individual measurement devices (flow meter, timer, volume measurement, pipette, collection efficiency). The random error was 13%, which corresponds to two times the standard deviation to have a confidence level of 95% assuming a normal distribution of the measurement values. Therefore, the overall uncertainty is thus 14%.

3.2.3.2 Effect of temperature on chromium evaporation

The Figure 9 illustrates the results from chromium evaporation measurements at 650, 700 and 750 °C in triplicates. The measured values are compared to value calculated from thermodynamic data, assuming that the equilibrium pressure is reached in the pipe. The three thermodynamics datasets are generated from three different experimental studies and they were obtained from Stanislawski et al. [58]. The experimental results of chromium evaporation obtained with the method presented here are coherent with the thermodynamic data found in the literature. In addition, the good repeatability of the method is demonstrated by the low standard deviation.

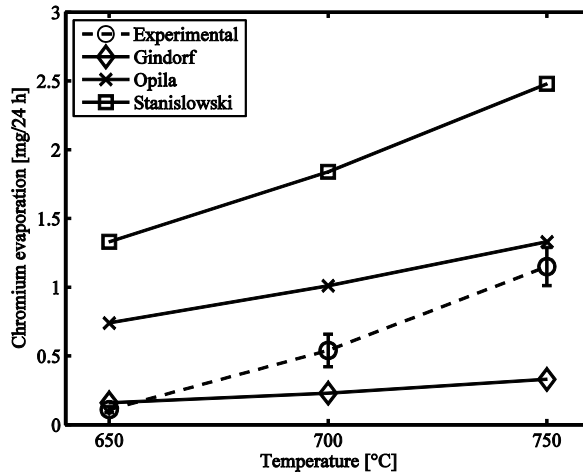


Figure 9. Measured amounts and standard deviations of evaporated Chromium at different temperatures. The experimental data are compared with calculations based on thermodynamics data from different sources (data extracted from [58]).

3.2.3.3 Effect of heat treatment history on chromium evaporation

It was found that the temperature history has a significant effect on the amount of chromium evaporation at 750 °C. A heat treatment of the pipe for 100 h at 800 °C resulted in a reduction by a factor of four in the volatile chromium concentration in the air exiting the pipe at 750 °C (from 8.0×10^{-8} to 2.0×10^{-8} kg m⁻³). To investigate the reason behind the decrease in chromium evaporation, the oxide layer on top of the stainless steel was investigated by SEM cross-section and EDS elemental mapping before and after the heat treatment. For this purpose, one pipe was exposed at 750 °C for about 300 h. Another pipe was exposed in a same way, except that it was subsequently exposed to 800 °C for 100 h before repeating the chromium evaporation measurements at 750 °C.

Figure 10 (a) and (b) present SEM micrographs of cross-sections of the inner surface of the stainless steel pipe before and after the exposure at 800 °C. Before exposure at 800 °C, a thin oxide layer of about 1 µm is present on the steel surface (Figure 10 (a)) and the oxide layer is chromium-rich (Figure 10 (c)). After exposure at 800 °C, the oxide layer was found to be about 10 µm thick (Figure 10 (b)) and its oxide layer is not homogenous in composition. The inner layer is chromium-rich and the top layer is depleted in chromium (Figure 10 (d)), but rich in iron oxide.

The reduction of chromium evaporation is explained by a thicker oxide layer, which is depleted from chromium at its surface. Enrichment in iron of the stainless steel oxide layer is associated with high oxidation rate because iron oxide is not as

protective as chromium oxide. Thus this is not beneficial for SOFC applications despite the associated reduction in chromium evaporation.

Although the reason for the formation of such an oxide layer is not ascertained, this result is presented here to illustrate the ability of the developed measurement method to notice an unexpected oxide layer growth through change in chromium evaporation rate. Alloy 253MA, the alloy of the pipe, is designed to withstand higher temperature and therefore this corrosion behaviour is unexpected.

The method presented here was used to quantify the chromium concentration at the outlet of a stainless steel pipe and it proved to be an effective tool because of its repeatability and the coherence of its results with thermodynamic data. In addition, it was sensitive enough to detect a heat treatment induced decrease in evaporation rate caused by an oxide scale growth. The method therefore fulfils its purpose and can be used to measure chromium evaporation from BoP component such as heat exchanger. The results presented here also confirm that stainless steel BoP components can contribute to the chromium intake of the stack, since the air exiting the investigated pipe was saturated with volatile chromium species.

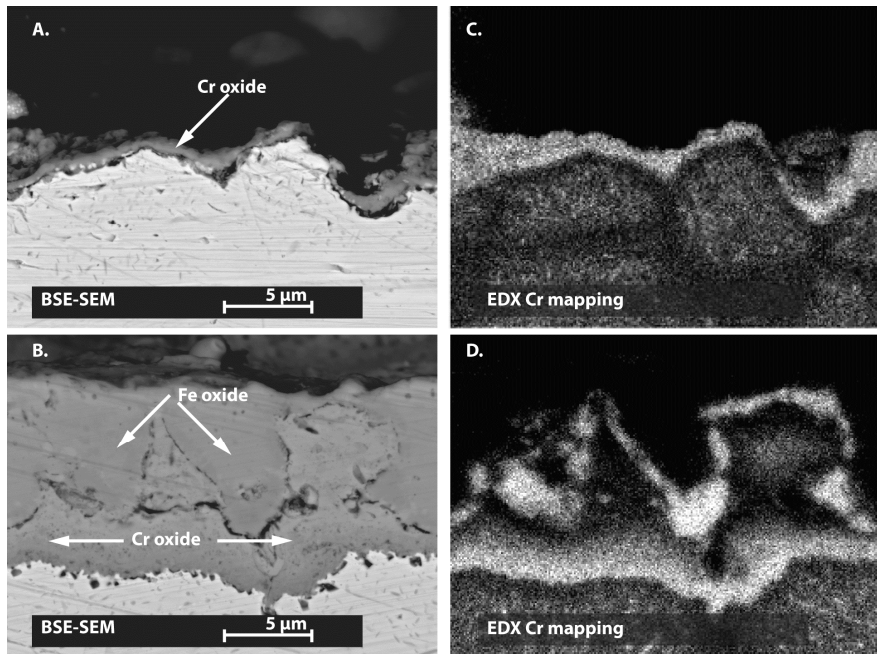


Figure 10 (a) and (b). SEM-BSE cross-section of the stainless steel before and after the 800 °C heat treatment. (c) and (d) EDX chromium mapping of the corresponding views.

4. Fuel processing subsystem

4.1 Effect of Anode off-gas Recycling on the pre-reformer (Publication III)

4.1.1 Background

The present chapter presents a study (Publication III) aiming at implementing an anode off-gas recycling loop in an SOFC system. An SOFC system that operates on steam-reformed fuel relies on a continuous supply of steam. It is technically simple to provide the steam from an external water supply with a deionisation system and an evaporator. However, this approach has significant drawbacks: the water source, the deionisation system and evaporator increase the system complexity and its maintenance requirements. Alternatively, the steam produced by the electrochemical reaction on the anode side (Equation 1) can be recycled back to the fuel inlet. It can be realised by recycling a fraction of the SOFC anode off-gas back to the fuel inlet. Thus, the need for an external water source is made unnecessary at least during operation [94]. Another significant advantage of recycling the anode off-gas is to increase the system efficiency. Because not all the fuel is utilised when it passes through the SOFC stack, recycling a part of this unreacted fuel allows to decrease accordingly the fuel inlet feed, which can improve the electrical efficiency of the system [95,96]. Lastly, the stack fuel utilisation can be decreased when an AOGR loop is used, which has been shown to be beneficial for the stack durability [97].

In practise, the implementation of a hot AOGR loop (i.e. without steam condensation) has proven challenging. AOGR can be implemented by a recycling blower or by an ejector, but suitable components cannot be found off-the-shelf at the moment [95]. Another issue is the risk of carbon formation which can occur if not enough steam is recycled, i.e. if the recycling ratio is too low [98]. Moreover, the risk of carbon formation increases when higher hydrocarbons than methane are present in the fuel [54]. It is possible to predict the gas composition, temperature and possibility for carbon formation using thermodynamic equilibrium calculation. However, actual carbon formation eventually depends on the activity of the reforming catalyst. Therefore, experimental investigation of the catalyst and pre-reformer is needed to map the safe operating region without carbon formation. Lastly, there is little experimental data reported in the literature on the effect of AOGR on cata-

lyst activity. Peters et al. reported that AOGR caused a decrease of the activity of a nickel-based catalyst [99], conversely Nummela et al. reported that AOGR had no negative effect on the performance of another pre-reformer nickel catalyst [100].

As already mentioned, the recycling ratio should be sufficient to have carbon-free operation. However, it should not be too high either, because it means larger parasitic electrical loss associated with the AOGR blower. In addition, AOGR results in a dilution of the fuel at the anode, which decreases the cell voltage [96]. Therefore, the recycling ratio should be optimised to have carbon-free operation and minimise the parasitic loss and the voltage drop.

This study aimed at generating the necessary results to build a pre-reformer for a 10 kW SOFC system including an AOGR loop [43]. This work contributes to the field of fuel processing in SOFC system by assessing experimentally the effect of AOGR on the performance of a precious metal-based pre-reformer using natural gas as a fuel. The performance of the pre-reformer in AOGR conditions is compared against SR conditions. Additionally, the effect of varying the recycling ratio is evaluated to determine its effect on the performance and to identify the minimum recycling ratio that can be used safely in an SOFC system, i.e. corresponding to carbon formation-free operation. The effect of the degree of reforming in the pre-reformer on the thermal management of the stack is out of the scope of this work. The temperature of the stack can be managed either by adjusting the degree of reforming of the pre-reformer or by adjusting the air flow and its temperature to the cathode. Results of this work led to the successful implementation of an anode off-gas recycling loop in a 10 kW SOFC demonstration unit, where the system is operated at nominal conditions without external water supply [43].

4.1.2 Experimental

The effect of AOGR on a precious metal catalyst-based pre-reformer was investigated in a natural gas pre-reformer test bench. As illustrated in Figure 11, the test bench consisted of the gas and deionised water mass flow controllers (EL-FLOW and LIQUI-FLOW, Bronkhorst), a water evaporator and mixer (CEM-303, Bronkhorst), a superheater (in-house built), a pre-reformer containing a commercially available precious metal catalyst monolith (Süd-Chemie), micro-quartz particle filters (MK 360, Munktell, designed to collect particles above 0.3 μm of diameter) and a heat exchanger (Alpha-Laval) to condensate the water from the exhaust gas. The temperature of the process gas was measured after the evaporator (TI1 in Figure 11), at the reactor inlet (TI2), at the catalyst monolith leading surface (TI3), at the centre of the monolith (TI4), at the trailing edge of the monolith (TI5), at the pre-reformer outlet (TI6), and after the filter (TI7). The process gas pressure was measured before the evaporator (PI1), at the pre-reformer inlet (PI2) and outlet (PI3) and after the filter (PI4). The dried pre-reformer exhaust gas was analysed by an online gas analyser (Sick S710 series) and with gas chromatographs (Agilent 6890 N, Agilent 6850 and HP 5890 Series II).

The heat used in the reforming reaction was supplied by heating the inlet gas in the superheater and the pre-reformer was used in a condition close to adiabatic, which means that heat loss was minimised by thermal insulation and electric heaters.

Depending on the pre-reformer temperature and gas composition, carbon formation can take place in the pre-reformer. The detection of its formation is based on pressure measurements. The carbon can accumulate on the catalyst surface and eventually cause a measureable increase of pressure at the pre-reformer inlet. Alternatively, the carbon formed in the pre-reformer can be carried downstream by the gas flow and is then collected at the filter, causing a measureable pressure increase before the filter. Additionally, when the pre-reformer was kept for an extended time in a defined condition, the set-up was flushed with nitrogen and air and the CO and CO₂ fractions at the set-up outlet were monitored to detect oxidation of possible carbon deposits.

The recycling gas compositions were synthesised using gas cylinders of carbon monoxide, carbon dioxide and hydrogen, in addition to deionised water (Millipore Elix system) and natural gas from the grid. The natural gas in the Finnish grid contains mainly methane (ca. 98%) with a small fraction of ethane, propane and nitrogen as listed in Table 1. The natural gas was desulphurised before the set-up with sulphur adsorbent (Süd-Chemie) because it contains 4–10 ppm of tetrahydrothiophene (THT) as an odorant.

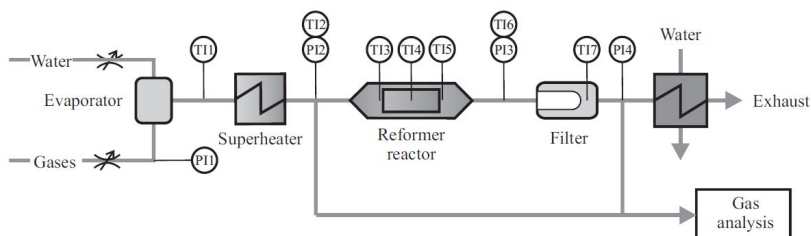


Figure 11. Schematic layout of the test equipment.

In order to assess the effect of an AOGR loop in an SOFC system on the pre-reformer, the pre-reformer was operated in two different modes. Firstly it was operated in steam reforming mode, in other words, only natural gas and steam were supplied to the pre-reformer. Secondly, natural gas was fed to the pre-reformer in addition to the simulated anode off-gas containing steam, carbon monoxide, carbon dioxide and hydrogen. This second mode is referred further as AOGR mode. In both cases, the pre-reformer inlet temperature was kept at 600 °C. The different experimental conditions are listed in Table 3. In steam reforming mode, the steam-to-carbon ratio (H₂O/C) was varied between 1.5 and 2.5. In AOGR mode, the recycling ratio varied between 0.2 and 0.7. The outlet gas of a correctly designed pre-reformer should be at thermodynamic equilibrium. There-

fore, the measured outlet gas temperatures and compositions are compared to the calculated equilibrium values to assess the performance of the pre-reformer.

The gas compositions given in Table 3 have been calculated on the basis of equilibrated gas with an in-house developed code [96]. Because this study aimed to generate the necessary results to build a pre-reformer for a defined SOFC system [43], the boundary conditions were predefined. In the calculations, the stack outlet temperature (700 °C), the stack fuel utilisation (0.6) and the current density were kept constant. Based on the heat exchanger layout (see Figure 2), the pre-reformer inlet temperature was expected to be about 600 °C in nominal conditions.

An important parameter for the pre-reformer operation is the gas hourly space velocity (GHSV), which is calculated by dividing the gas volume flow ($\text{Nm}^3 \text{h}^{-1}$) at normal temperature and pressure (NTP) by the catalyst volume (m^3). On the one hand, it is advantageous to operate the pre-reformer at as high a GHSV as possible, since it minimises the pre-reformer size, the amount of expensive catalyst material and the pressure drop at the pre-reformer. On the other hand, the GHSV should be limited to a value at which the gas reaches thermodynamic equilibrium at the pre-reformer outlet. A GHSV value of about $20,000 \text{ h}^{-1}$ at recycling ratio of 0.5 was selected as a reference condition in this study. The GHSV was chosen based on previous experience with this catalyst and the recycling ratio is based on the results of an electrical efficiency optimisation study. The GHSV corresponding to the different experimental conditions is plotted as a function of the recycling ratio in Figure 12 (left). It can be noted that the GHSV increases with the recycling ratio, which means that the residence time of the gas in the pre-reformer becomes shorter. Additionally, the natural gas inlet flow rate is also plotted as a function of the recycling ratio in Figure 12 (right) and it can be seen that the natural gas flow rate decreases when the recycling ratio is increased, illustrating how much fuel can be saved by increasing the recycling ratio.

Table 3. Experimental conditions in SR and AOGR modes.

	H ₂ O/C	Recycling ratio	GHSV (h ⁻¹)	NG	CO	CO ₂	H ₂	H ₂ O	Methane conversion (%)
SR	2.5	–	21 900	28.6	0	0	0	71.4	17
	2	–	18 800	33.3	0	0	0	66.7	15
	1.5	–	15 700	40	0	0	0	60	13
AOGR		0.2	10 200	56.7	5.5	8.8	14.1	14.8	5
		0.28	12 100	46	6.4	11.6	16.5	19.5	5
		0.36	14 500	37.1	6.9	14	17.9	24	6
		0.4	15 800	33.3	6.8	15.3	18.1	26.4	7
		0.5	20 000	25	6.7	18.3	17.9	32.2	9
		0.55	22 700	21.5	6.4	19.8	17.4	35	11
		0.6	26 100	18.2	6	21.2	16.5	38	13
		0.65	30 300	15.3	5.5	22.7	15.4	41.1	16
		0.7	35 800	12.5	5	24.1	14.1	44.3	19

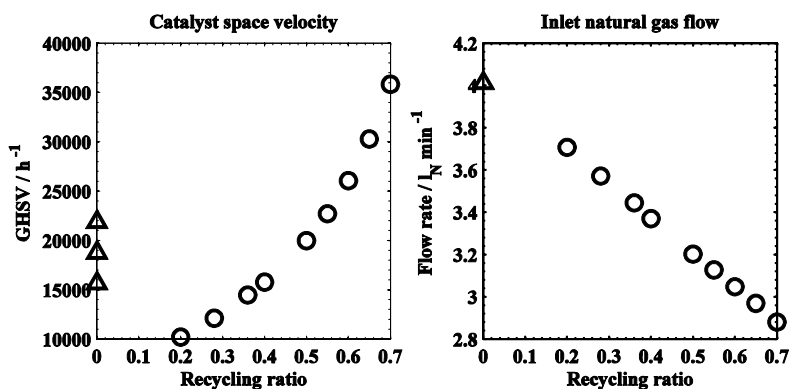


Figure 12. GHSV of the pre-reformer catalyst and the inlet natural gas flow rate in SR (Δ) and AOGR (\circ) modes for different recycling ratio values.

The temperature limits of carbon formation in AOGR mode were calculated using HSC6.1 [92] software to assess which experimental conditions could potentially

lead to carbon formation in the pre-reformer. The equilibrium temperature and composition of the pre-reformer outlet gas were calculated with the Cantera toolbox [101] using GRI-Mech 3.0 reactions developed for natural gas combustion [102]. The equilibrium was solved for an adiabatic system, where the total enthalpy and pressure between reactants and products was kept constant.

In addition to short-term experiments, the pre-reformer was held in selected conditions for a longer period to observe possible carbon formation or degradation of the catalyst performance. The conditions of the different holds are detailed in Table 4 and the longest hold was 1000 h.

Table 4. Operation conditions during extended holds.

Hold no.	Recycling ratio (-)	Inlet temperature (°C)	GHSV (h ⁻¹)	Hold time (h)
1	0.6	609	26,100	122
2	0.5	597	20,000	121
3	0.5	598	20,000	117
4	0.5	513	20,000	67
5	0.5	600	20,000	1000
6	0.2	589	10,200	165
7	0.2	646	20,300	165

4.1.3 Results and discussion

4.1.3.1 Risk of carbon formation at thermodynamic equilibrium

In order to evaluate the effect of AOGR on the performance of a precious metal-based catalyst, a pre-reformer was operated with simulated conditions relevant to an SOFC system using steam-reformed natural gas, with or without an AOGR loop. First of all, the risk of carbon formation was investigated and the carbon formation limits based on thermodynamic calculations are illustrated in Figure 13. According to thermodynamic equilibrium, the risk of carbon formation is more severe at a lower recycling ratio. This stems from the O/C value (also shown in Figure 13) which decreases with the recycling ratio, in other words, when less steam and other oxygen-containing species from the anode outlet are recycled back to the pre-reformer inlet. At a recycling ratio of 0.5, the calculated temperature limit of carbon formation is already below the typical operating temperature of anode-supported SOFCs (700–800 °C). However, the pre-reformer temperatures are typically lower, e.g. between 500 and 600 °C depending on the system layout; therefore there is a higher risk of carbon formation in the pre-reformer compared to the SOFC stack. Carbon is stable in equilibrium conditions at a typical operating temperature of a pre-reformer below a recycling ratio of about 0.65. The risk of

carbon formation was further assessed experimentally, as described below in Section 4.1.3.3. The experimental conditions tested in this work are illustrated in Figure 13 in the red rectangle.

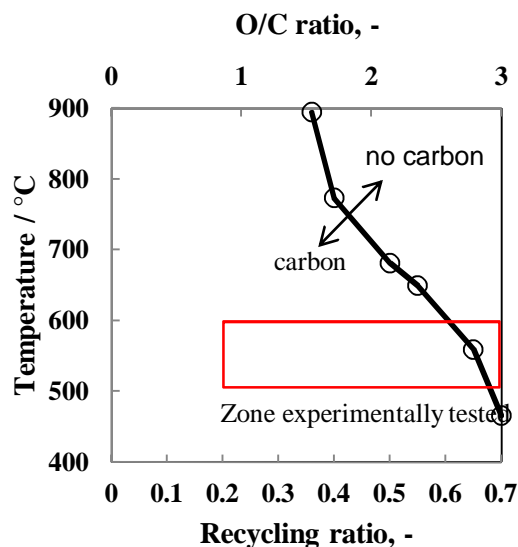


Figure 13. Temperature limit of carbon formation based on thermodynamic calculations in AOGR mode with a varying recycling ratio. The corresponding O/C ratios are shown in the secondary x-axis. The red rectangle shows the limits of the experimental conditions tested in this work.

4.1.3.2 Effect of AOGR on the performance of the pre-reformer

The performance of the pre-reformer and the catalyst were then tested by comparing the measured outlet temperature and gas composition with the values obtained by thermodynamic calculations. The inlet and outlet temperature of the pre-reformer are illustrated in Figure 14 in steam reforming and AOGR modes and the measured outlet temperature is compared to the calculated equilibrium outlet temperature. The difference between the experimental and equilibrium outlet temperature is larger in steam reforming mode compared to AOGR mode; this indicates that the equilibrium is not reached in steam reforming mode. This is also confirmed by the comparison of the experimental and equilibrium outlet gas fractions of methane and hydrogen in Figure 15. There is a systematic deviation from equilibrium values for the methane and hydrogen fractions in steam reforming mode, whereas experimental and equilibrium values are within the error limits in AOGR mode. Because both the outlet temperature and methane fraction are higher than the equilibrium values, kinetics is probably limiting the extent of the SR

reaction. In other words, to achieve equilibrium with this inlet gas composition and temperature, the GHSV should be reduced. Conversely, in AOGR mode, the equilibrium is reached regardless of the recycling ratio.

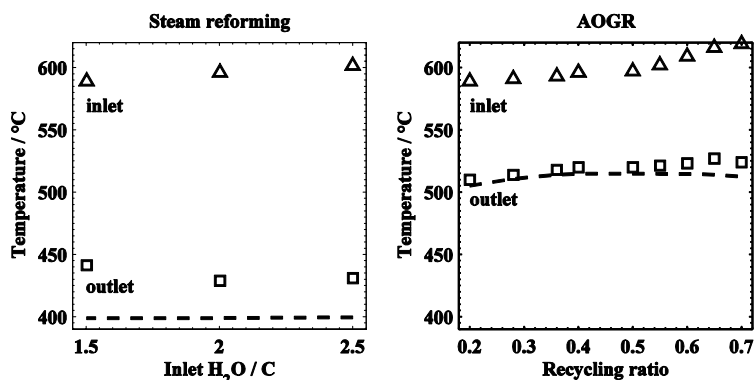


Figure 14. Inlet and outlet temperature of the pre-reformer in SR and AOGR modes. Δ : measured inlet temperature, \square : measured outlet temperature, dashed line: calculated equilibrium temperature.

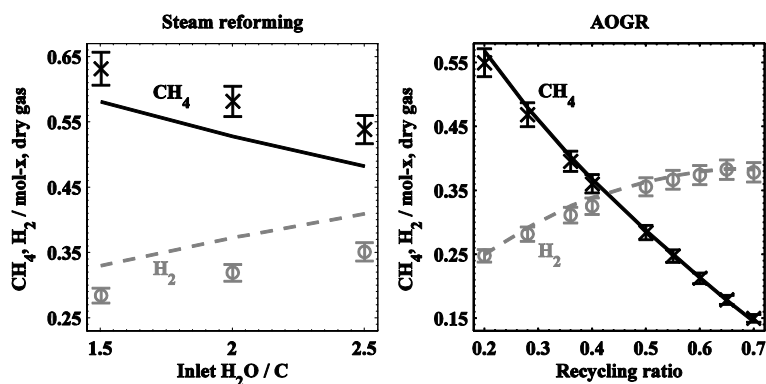


Figure 15. Molar fraction of methane and hydrogen at pre-reformer outlet with varying SR and AOGR conditions. Measured values are x: methane and o: hydrogen. Calculated equilibrium values are solid line: methane and dashed line: hydrogen.

In order to investigate possible limitations with regards to the GHSV in AOGR mode, the pre-reformer was tested with a fixed gas composition corresponding to a recycling ratio of 0.5 and with varying the GHSV from 20,000 to 35,000 h^{-1} , which is the maximum value achievable in this set-up. The methane and hydrogen fractions at the outlet as a function of GHSV are illustrated in Figure 16. The experimental values exhibit no deviation from the equilibrium values, which means that there is no kinetics limitation in the tested range of GHSV in AOGR mode.

The results show that equilibrium is more readily achieved in the pre-reformer tested using AOGR mode compared to SR mode. In other words, implementing an AOGR loop in the considered SOFC system enables a reduction in the size of this precious metal catalyst compared to the steam reforming case. This result contrasts with the conclusions of Peters et al., who reported that the use of AOGR caused a decrease in the activity of a nickel-based catalyst in AOGR conditions [99]. The difference between the results obtained by Peters et al. and those presented here probably originates from the catalyst used, nickel-based versus precious metal-based catalyst. Moreover, the catalyst can be used at high GHSV (at least up to 35,000 h⁻¹) without kinetics limitation at an inlet of 600 °C. As a comparison, nickel-based catalysts have been used at a much lower space velocity, in the range of 2000–6000 h⁻¹ [100].

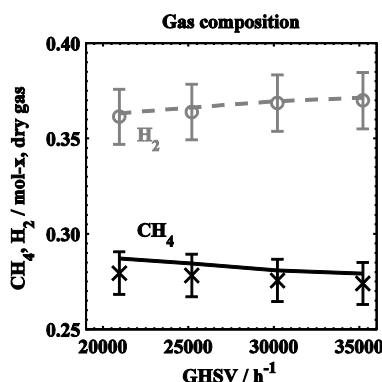


Figure 16. Molar fraction of methane and hydrogen at the pre-reformer outlet in AOGR mode with varying GHSV at recycling ratio of 0.5. x: methane, and O: hydrogen. Calculated equilibrium values are presented with lines.

4.1.3.3 Carbon formation during extended holds

The pre-reformer also operated in selected conditions for longer time (see Table 4) to investigate possible carbon formation in the pre-reformer or change of catalyst performance. For this purpose, the pre-reformer outlet temperature, gas composition and pressure drop over the catalyst and filter were monitored during the hold. Additionally, after each hold, the set-up was flushed with nitrogen and air and the CO and CO₂ fraction at the set-up outlet was monitored to detect oxidation of possible carbon deposits. It should be noted that carbon is present at the thermodynamics equilibrium for all the conditions tested in Table 4 (see Figure 13).

The measured and calculated pre-reformer outlet temperature and methane fraction during the long-term holds are illustrated in Figure 17. It shows that there are no significant changes in outlet temperature and composition during the different holds. Moreover, the measured values are close to the calculated equilibrium

values. It is only during the last hold that an increase in the methane fraction is measured. However, in this condition, the gas composition corresponded to a recycling ratio of 0.2 and it is unlikely that such a low recycling ratio would be used in an actual system without an external steam supply because of the risk of carbon formation in the SOFC stack (see Figure 13).

Similarly to the outlet temperature and methane fraction, the pressure drop over the pre-reformer reactor did not change significantly during the holds with a variation of less than 1 mbar observed. This method is not very sensitive to a small amount of carbon. However, if equilibrium was reached, the amount of solid carbon expected would be about 50 g per hour at a recycling ratio of 0.5, which would certainly be detected in less than an hour. Moreover, the oxidation procedure carried out after each hold did not reveal any carbon accumulation at the reactor (detection limit of the order of 1 mg). These results indicate that carbon formation is not taking place to an extent that would compromise the operation of this pre-reformer in an SOFC system with the tested recycling ratios, even though carbon is present at thermodynamic equilibrium. This result is significant because it enables the optimisation of the system's operation and the minimising of the losses associated with a high recycling ratio. Additionally, they confirm that the experimental evaluation of the catalyst in the conditions of interest is needed to assess the actual risk of carbon formation.

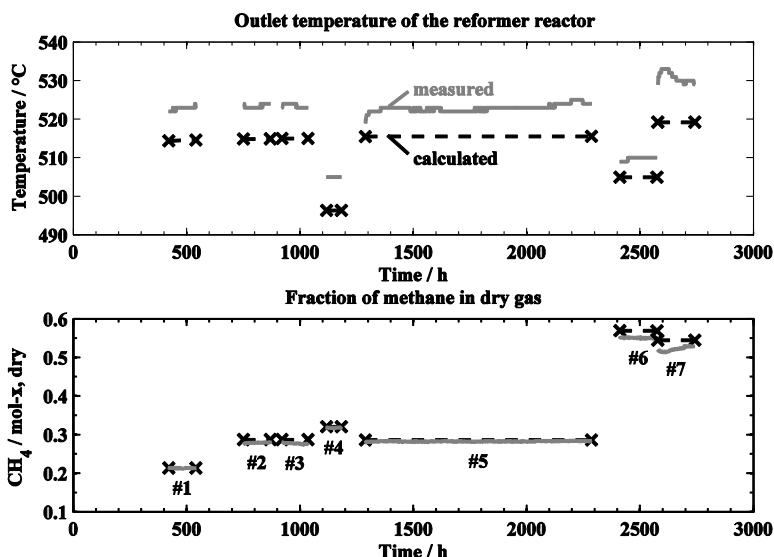


Figure 17. Temperature (above) and molar fraction of methane (below) at a reactor outlet during the experiment. The measured value is presented by a solid line and the calculated equilibrium value by a dashed line with markers at the ends.

The aim of this study was to generate the results necessary for the implementation of an AOGR loop in a 10 kW SOFC system. The main results are that the outlet gas of the tested pre-reformer and catalyst reach thermodynamic equilibrium more readily in AOGR conditions compared to SR conditions. No deviation from equilibrium was observed with a GHSV of 35,000 h⁻¹ and a recycling ratio of 0.5. Lastly, carbon formation was not observed during long-term holds (up to 1000 h), despite carbon being stable at equilibrium in the tested conditions. Therefore, the pre-reformer and catalyst are considered suitable for implementation in a 10 kW system including an AOGR loop.

4.2 Generation of anode protective gas with the system pre-reformer (Publication IV)

4.2.1 Background

Commonly, SOFC anodes are made of a nickel cermet, where the particles of nickel are in their metallic form during operation. However, nickel can oxidise if the stack is hot (> ca. 300 °C) and no reducing gas is fed to the anode. The oxidation of nickel is very detrimental because it causes a loss of catalyst activity and a volume increase. Even if the nickel can be reduced again, the volume change causes mechanical stress and affects the durability of the stack [103]. Tolerance to reoxidation cycles depends on the microstructure and mechanical properties of the cells, and efforts are made to develop cells with improved tolerance [104,105]. Alternatively, it is possible to design and operate the BoP components of the SOFC system to avoid the conditions leading to nickel oxidation; in other words, to ensure that there is a reducing atmosphere when the stack is above ca. 300 °C. A critical time is the heat-up of the system, which might last several hours from room temperature to operating temperature (600–800 °C) in order to keep the thermal gradient and thermal stresses at an acceptable level. Nickel cermet anode was observed to start to oxidise at temperatures as low as 290 °C [106] and the oxidation kinetics increases with temperature [107]. Air can be present on the anode side because of the transport from the cathode to the anode side through the electrolyte or stack seals [108] and air might have migrated to the anode side from the exhaust when the system was shut down. Therefore, a forced flow of reducing protective gas is necessary during heat-up to displace the oxygen and maintain reducing conditions at the anode.

As explained in Section 4.1, SOFC systems that include an AOGR loop achieve higher efficiencies and potentially simpler design compared to an SOFC system without AOGR [109]. However, the AOGR loop needs to be operating during the heat-up phase in order to heat up all the system components. As a consequence, the air that leaks to the anode side is force-fed back to the pre-reformer inlet, which increases the risk of anode reoxidation.

The simplest and safest way to protect the anode during heat-up consists of using premixed protective gas such as 4%-vol hydrogen in nitrogen. This approach is not practical for commercial applications because such premixed protective gas is expensive and due to the lengthy heat-up time, a relatively large amount is needed. For example, five cylinders of 50 L at 200 bars would be needed to heat up and start up the 10 kW demonstration unit [43]. Lastly, the protective gas cylinders require space and their replacement and logistics add up to the operation and maintenance costs. There is therefore a clear incentive to produce such protective gas within the SOFC system and it can be accomplished by reforming natural gas in the pre-reformer by providing the steam with the start-up steam generator. The challenge consists of operating the pre-reformer at a sufficiently high temperature for the catalyst to be active for steam reforming while avoiding carbon deposition in the pre-reformer and at the anode during heat-up. Additionally, carbon-containing species can form nickel carbonyl at the anode below 230 °C according to reference [105] and the toxicity of this gas is extremely high (the lowest published lethal concentration for humans is 30 ppm for 30 min [110,111]; therefore, the conditions for its formation should be strictly avoided.

Publication IV presents a study aiming at developing a method to heat up the 10 kW demonstration unit without premixed protective gas using natural gas and steam. Firstly, ex-situ experiments were conducted on a pre-reformer test bench. The aim of these experiments was to realise the suitable operating parameters of a pre-reformer at low temperature (<500 °C) in a system with an AOGR loop and air leakage (i.e. forced oxygen supply to the fuel system). Secondly, the results of the ex-situ experiments were used to develop a safe heat-up procedure for a 10 kW SOFC system without the use of premixed protective gas. A series of heat-up cycles were performed on the SOFC system and the performance of the stack was investigated after each heat-up. Several authors have investigated the heat-up of an SOFC by modelling [103,112,112-114], but at the time of writing, no experimental work describing the heat-up of a planar SOFC system with AOGR had been published previously.

4.2.2 Experimental

4.2.2.1 Ex-situ pre-reformer experiments

The ex-situ experiments were performed on a pre-reformer test bench described in Figure 11 in Section 4.1.2. The aim of these experiments was to assess the activity of a precious metal monolith catalyst at low temperature in natural gas steam reforming. The light-off temperature was determined by the pre-reformer inlet gas temperature at which the pre-reformer starts to convert methane to hydrogen according to the steam reforming reaction (Equation 4).

The gas outlet composition was monitored continuously with an online gas analysis equipment (IR-based for CH₄, thermal conductivity for H₂ and paramag-

netic for O₂, Sick Maihak S700 series). The analyser results should be used to evaluate trends rather as quantitative measurements because of the different channels' cross-sensitivity. The temperature of the inlet gas was ramped up from 200 to 550 °C at a rate of about 2 °C min⁻¹. The GHSV of the pre-reformer was about 32,000 h⁻¹. The investigated inlet gas flows are listed in Table 5. These conditions are relevant to the gas composition of an SOFC system using AOGR, when the steam and fuel supply have just been initiated and the temperature is too low to expect reforming activity in the pre-reformer or in the stack. Without reforming, the gas in the recirculation loop consists of natural gas, steam and the air originating from stack leakages. The gas composition in run 1 includes only natural gas (98% methane), steam and nitrogen. This is the zero-leakage case. In runs 2–7, a small fraction of air was added to simulate the effect of air leakage on the activity of the pre-reformer. In runs 3–7, hydrogen was added with varying H₂/O₂ ratio from 0 to 4 according to Equation 19.



Nitrogen was added to all runs because a sufficient flow of carrier gas is needed to operate the steam evaporator and mixer (CEM-303, Bronkhorst). Nitrogen is not expected to react in the tested conditions.

Table 5. Test gas mixtures used for determining the light-off temperature.

Run		1	2	3	4	5	6	7
Gas flow / NLPM	NG	0.5	0.5	0.5	0.5	0.5	0.5	0.5
	H ₂ O	10	10	10	10	10	10	10
	N ₂	10	10	10	10	10	10	10
	H ₂	-	-	0.2	0.05	0.1	0.15	0.4
	Air	-	0.5	0.5	0.5	0.5	0.5	0.5
H ₂ /O ₂			0	2	0.5	1	1.5	4

4.2.2.2 System heat-up experiment

The experiments at system level were realised with the 10 kW demo unit, which is described in Section 2.5 and illustrated in Figure 2. The system included a 10 kW stack consisting of 64 anode-supported cells (Versa Power Systems [115]). The heat needed for the system heat-up was primarily provided by the electrical heater located at the stack air inlet inside the module, and secondarily heat-up was assisted using an electric heater in the AOGR loop.

Based on the results obtained from the ex-situ pre-reformer tests, a heat-up procedure was developed that would not use any premixed protective gas. The heat-up procedure is illustrated in Figure 18 and consists of four phases.

1. The stack is heated up from room temperature to over 200 °C and all the other fuel subsystem components to at least 100 °C, without any forced flow to the system fuel inlet. The cathode air blower and the AOGR blower are in operation throughout the entire heat-up procedure.
2. Steam is introduced to the fuel side using the steam start-up generator when the stack temperature is above 200 °C. The natural gas was fed in only when the stack temperature was above 300 °C to avoid the risk of formation of toxic nickel carbonyl in the SOFC stack. Pre-reformer light-off was triggered by a short-term hydrogen pulse.
3. The stack is heated up to a temperature of 700 °C. The anode is protected from reoxidation by the hydrogen produced by the natural gas steam reforming reaction.
4. The electrical loading of the stack is started and the fuel is proportionally increased. When sufficient steam is produced in the stack, the external steam supply is stopped.

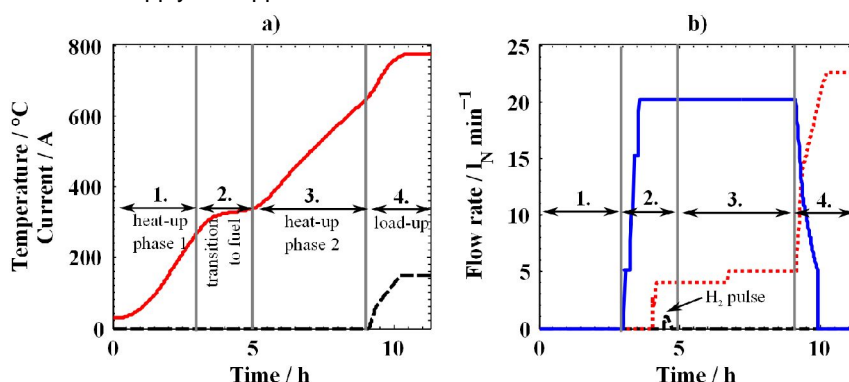


Figure 18. Experimental start-up. (a) Stack temperature (solid line) and current (dashed line) (b) Flow rate of hydrogen pulse (dashed line), fuel (dotted line) and steam (solid line).

4.2.3 Results and discussion

4.2.3.1 Ex-situ pre-reformer experiments

The activity of a precious metal catalyst in steam reforming was investigated at a low temperature on an ex-situ pre-reformer. Figure 19 illustrates the outlet gas composition against the inlet temperature of the pre-reformer for the different investigated runs, see Table 5. In Figure 19 (a), it can be seen that the catalyst

exhibits some measureable activity at 235°C with the inlet gas from run 1 (zero-leakage case). The methane conversion increases gradually with the inlet temperature. The inlet temperature at which the methane conversion starts is further referred to as the light-off temperature. In Figure 19 (b), some air is added to the inlet gas to simulate the effect of air leakage in the system (run 2). Conversely to the “zero-leakage case”, the catalyst exhibits no activity before its inlet reaches ca. 390 °C. Above this temperature, the reforming reaction starts abruptly and then methane conversion increases gradually. Apparently, the presence of oxygen has an inhibiting effect on the tested catalyst at low temperatures. In Figure 19 (c), hydrogen is added at a stoichiometric ratio with oxygen (run 3) and methane conversion is already observed at 200 °C. Apparently, the combustion of hydrogen (Equation 19) occurs at 200 °C, which removes the inhibiting effect of oxygen and increases the temperature in the catalyst. Qualitatively, this result is similar to the one obtained in run 1 (Figure 19 (a)), in other words, the methane conversion starts at as low a temperature as around 200 °C.

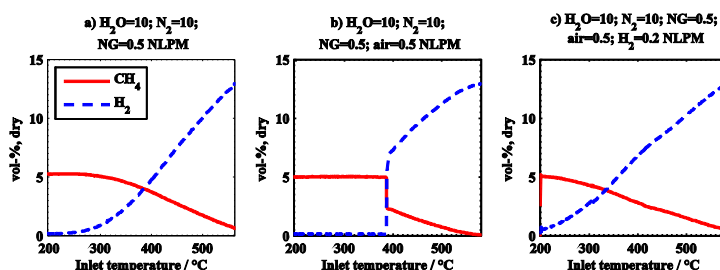


Figure 19. Pre-reformer dry outlet gas composition against pre-reformer inlet gas temperature. (a) Fuel and steam (zero-leakage case, run 1), (b) addition of air (run 2) and (c) addition of air and hydrogen at stoichiometric ratio (run 3).

Figure 20 illustrates the effect of different H₂/O₂ ratios in the inlet gas on the light-off temperature of the pre-reformer. With no hydrogen present, the light-off temperature is as high as ca. 390 °C, the light-off temperature then decreases when the H₂/O₂ ratio is increased. At a H₂/O₂ ratio of two (stoichiometric ratio of equation 19), the light-off temperature is below 200 °C. These results indicate that the steam reforming of methane can be triggered in two ways during the heat-up of an SOFC system: either to increase the temperature of the pre-reformer inlet to about 400 °C in order to overcome the inhibiting effect of oxygen originating from leakages, or to add a relatively small amount of hydrogen to decrease the light-off temperature to below 200 °C. From a system point of view, it is beneficial to be able to reform the natural gas to hydrogen-containing reformat as early as possible during the heat-up procedure. If hydrogen can be generated before the temperature of the anode is above 300 °C, the need for premixed protective gas to protect the anode from reoxidation can be completely suppressed. These results are further exploited to design a procedure to heat up an SOFC system without the use of premixed protective gas.

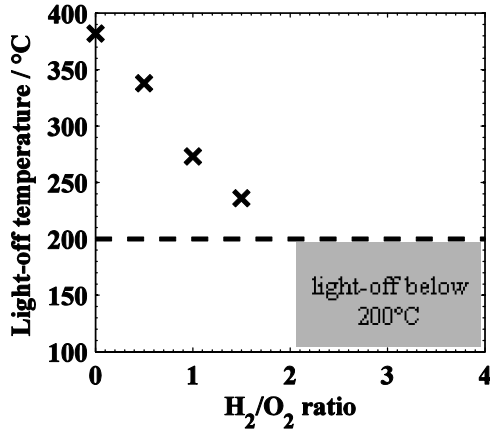


Figure 20. The effect of the H₂/O₂ ratio on the light-off temperature of the pre-reformer, results from runs 2–7.

4.2.3.2 System heat-up experiments

The heat-up of the 10 kW demo unit was experimentally investigated and a selection of the results is depicted in Figure 21. It should be noted that the anode inlet concentration (Figure 21 (c)) also corresponds to the pre-reformer outlet concentration. During the first phase, the stack was heated up until ca. 350 °C (Figure 21 (a)). The anode inlet concentration was about 21% oxygen, meaning that mostly air was present in the fuel system (Figure 21 (c)). At $t = 4$ h, the oxygen concentration decreased by about 1%, when the stack temperature was between ca. 200 and 350 °C, which is explained by the slow start of the oxidation of nickel at the anode. During the second phase, 20 NLPM of steam feed was initiated when the stack was ca. 350 °C at $t = 4$ h. At $t = 5$ h, 4 NLPM of natural gas was fed into the system and the concentration at the anode inlet was measured to be about 50% methane and 8% oxygen, indicating that the amount of air leak to the fuel side was approximately of the same magnitude, i.e. 4 NLPM. The pre-reformer inlet and outlet temperature are very close (Figure 21 (b)), indicating that no reforming reaction is taking place at the pre-reformer between $t = 3.5 \dots 5.5$. This result is similar to that obtained in the ex-situ pre-reformer, where the reforming reaction is inhibited by the presence of oxygen under 400 °C. At $t = 5.5$ h, a short hydrogen pulse (15 minutes) is initiated and can be seen as a stack voltage increase (Figure 21 (a)) and by the increase of the pre-reformer outlet temperature, which means that hydrogen reacts with the oxygen that is present and is confirmed by the drop in oxygen concentration at the anode inlet. At the same time, a small amount of methane is converted and the hydrogen concentration at the pre-reformer outlet is about 2% after the termination of the hydrogen pulse. The third phase consists of resuming the heat-up of the stack to 700 °C. During $t = 5.5 \dots 6.5$ h, the pre-reformer catalyst activity is only slightly increasing. At $t = 6.5$ h, at a stack temper-

ature of about 400 °C, the nickel of the anode is reducing, the cell voltage increases suddenly and methane starts to be reformed in the stack, as seen in the large decrease of methane and increase of hydrogen concentration at the anode inlet. The fourth and final phase consists of electrical loading of the stack (not shown in Figure 21).

In short, the oxygen present on the fuel side during heat-up starts to partially oxidise the anode at temperatures below 350 °C and inhibits the steam reforming reaction at the pre-reformer. A hydrogen pulse is needed to remove this molecular oxygen by catalytic combustion with hydrogen on the precious metal catalyst of the pre-reformer and to start the production of a small amount of hydrogen in the pre-reformer. When the stack temperature increases further to about 400 °C, the nickel fraction of the anode that had oxidised is reduced and natural gas is reformed in the stack. The heat-up can proceed without excessive oxidation of the anode.

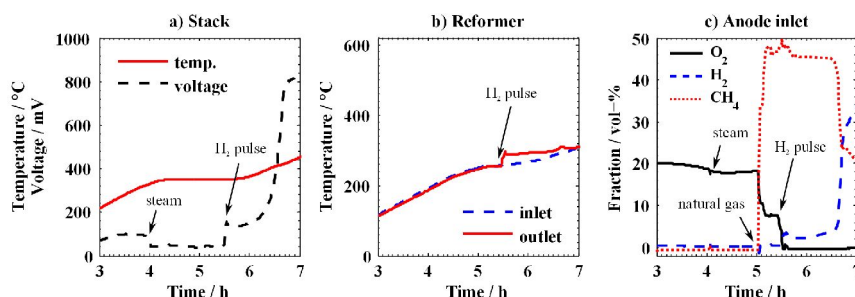


Figure 21. Heat-up of the 10 kW demo unit without premixed gas (a) stack temperature and average cell voltage, (b) inlet and outlet temperature of the pre-reformer (c) fraction of methane, hydrogen and oxygen at the anode inlet on a dry basis.

The cell voltage after experimental heat-up is used as an indicator of damage to the stack during the heat-up procedure. The difference in individual cell voltage at 150 A before and after two experimental heat-up procedures is depicted in Figure 22. Most of the voltage changes were small and within 10 mV for the majority of the cells and the average cell difference is below 1 mV. The result from the cell #64 is not considered because this cell was already severely degraded before the experimental heat-up procedures and its result are consequently not considered relevant. Therefore, the experimental heat-up without the use of premixed protective gas appears to have caused no measurable degradation to the stack. This result validates the possibility of producing the reducing protective gas inside the system at the pre-reformer using a hydrogen pulse. However, the results obtained from the ex-situ pre-reformer suggest that natural gas can be reformed in the presence of oxygen if the temperature of the pre-reformer inlet is above 400 °C. Therefore, the system could be further simplified by eliminating the hydrogen

pulse if the pre-reformer inlet gas could be heated up to above 400 °C when the stack is at about 350 °C.

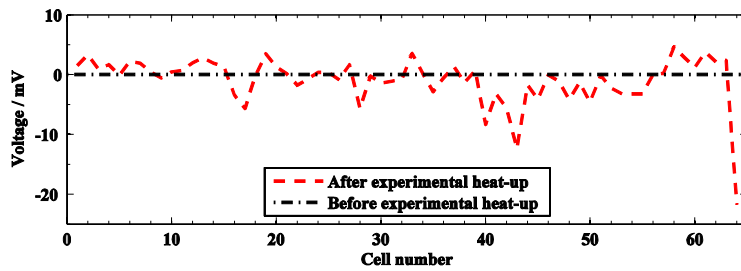


Figure 22. Difference in individual cell voltages after two experimental heat-up procedures.

5. Performance and material compatibility of hybrid seals (Publication V and VI)

5.1 Background

Compressive seals composed of mica-type paper have been investigated for SOFC stack applications [32,35,36]. They have the advantages of having good thermal cycling capability and being easy to handle during stack assembly [116]. However, they exhibit a relatively high leak rate, principally due to the presence of interfacial leak paths between the seal and adjacent stack components [37]. For this reason, they require high compressive stresses (usually at least 2 MPa) to decrease the extent of these interfacial leak paths for adequate sealing performance [35,36,117]. For example, in Publication I, the stack had a cell footprint of 100 cm² and the applied load on the stack was about 2000 kg, corresponding to about 4 MPa on the seals. Compression is needed in SOFC stacks to ensure adequate sealing performance when using compressive seals and good electrical contact between cells and interconnects. There are multiple benefits to reducing the compression requirement for the stack, such as reducing the compression system size and its complexity. Additionally, the compression rods usually need to go through the stack insulation; therefore, the thinner the rods, the smaller the heat loss. A smaller compression also enables the use of thinner and less robust stack components. This means that there are clear benefits to decreasing the compression stress needed on compressive seals, while retaining the easy handling and assembly of this type of seal.

To overcome the drawbacks of the compressive seals, hybrid seal concepts have been developed. The principle is to have a core made of compressible materials sandwiched between layers of compliant materials that would block the interfacial leak paths. Thus, the hybrid seal inherits its mechanical properties from the compressible core but exhibits a low leak rate, even at lower compression stresses. This enables the compressible core to deform in response to thermo-mechanical stresses without causing the failure of the seal. The hybrid seal concept has been investigated by Chou et al. using different micas for the compressible core and glass or silver foil as compliant layers [118-124].

In addition, it is essential that the sealing materials exhibit limited material interactions with the other SOFC stack components to ensure sufficient stack durability. Sealing material interaction studies have previously been published in the literature, on pure ceramic glass seals [62,125] or on compressible seals [126,127]. They observed different forms of accelerated corrosion that all took place preferentially at the three-phase interface sealing material/interconnect steel/air. Chou et al. presented a post-experimental analysis of a stack using hybrid seals [128]. They concluded that material interaction was limited and that their material selection for the seal and interconnect material was suitable for long-term operation. However, the three-phase interfaces between seal/interconnect/gas were not discussed.

The work presented here contributes to the field of sealing solutions for SOFC by presenting the hybrid seal development at VTT Technical Research Centre of Finland. The sealing solution uses Thermiculite 866 [129] as a compressible core coated with glass using an organic carrier. The advantages of using Thermiculite 866 over traditional mica-type paper are its improved gas tightness, because of the presence of steatite filler between the vermiculite platelets, and its superior compressibility [35]. The method presented here enables easy stack manufacturing because the seal can be coated beforehand, cut to shape and handled in the same way as traditional compressible gaskets. The organic carrier present in the glass coating is burned out in the first heat-up and the remaining glass forms a thin conformable interlayer between the seal core and adjacent stack components. The major advantage of the conformable core is also its ability to compensate for manufacturing tolerances of the adjacent components. Publication V presents the manufacturing method of the coated seals and the results from ex-situ leakage tests. The possible material interactions between seals and adjacent components have been investigated in Publication VI, where a post-experimental analysis of an SOFC stack using hybrid seals is detailed. The stack operated for 1800 h at 700 °C. The in-situ nature of the experiment provides exposure conditions to the seals and interconnects that are more relevant to stack operation compared to ex-situ experiments.

5.2 Experimental

5.2.1 Ex-situ leak rate measurement

The improvement brought about by adding compliant glass layers to compressive sealing materials was evaluated by leak rate measurements of seal samples made of Thermiculite 866 (Flexitallic Ltd) material, either uncoated or coated with glass layers. Thermiculite 866 is a commercial compressive material composed of vermiculite and steatite. The materials of the seal were selected to target operation at 700 °C. The glass used was a commercial glass with a softening temperature of 650 °C to obtain a compliant layer.

For the leak test experiments, Thermiculite 866 was coated by wet spraying. A fluid mixture of glass powder and organic carrier (24%-weight of Terpeneol, 75%-weight of ethanol and 1%-weight of ethyl cellulose) was prepared with a glass-to-organic ratio of 0.5 by weight. After coating, the coated substrate was cut to the required shape. All the seals were heated from room temperature up to 700 °C using a 1 °C min⁻¹ ramp rate.

The set-up used to measure the leak rate ex-situ is illustrated in Figure 23. Mass flow controllers fed gases to the sample line and exhaust line. The pressure inside the seal was controlled with a back pressure controller. During heat-up, air was fed to the seal samples to burn off the organic binders. The seal samples were ring-shaped with an outer diameter of 40 mm. The seal samples were placed on a 10 mm-thick Crofer 22 H bottom plate, from where the gas was fed to the samples. A 1 mm-thin plate of Crofer 22H was placed on top of the seal sample and weight plates were added on top of it. The measurement set-up mimics the conditions inside a stack by using the relevant test temperature, heat-up procedure, steel materials, hydrogen-containing gas and applied stress on the seal sample, but the measurement is qualified as ex-situ because it is not conducted inside a stack.

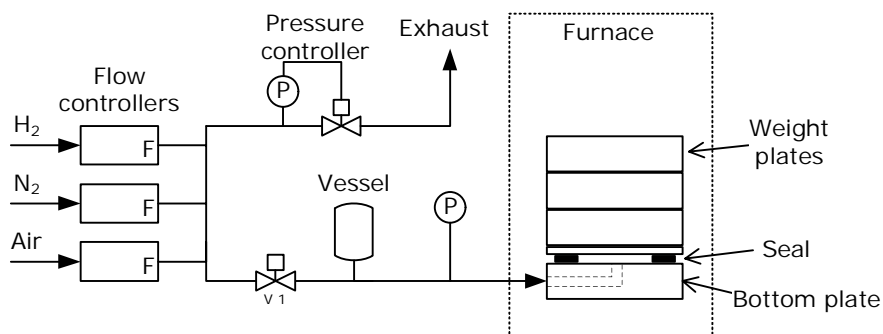


Figure 23. Measurement set-up for the ex-situ leak rate test.

After heat-up, the pressure inside the seal was set 25 mbar above ambient in a gas mixture of nitrogen and hydrogen at 700 °C. Leak rate measurements were performed periodically by shutting off valve V1 and measuring the pressure decay. A vessel of a known volume was connected to the sample line, enabling calculation of the leak rate as a function of pressure from the pressure decay curve. Based on the ideal gas assumption, the leak rate is proportional to the slope of the pressure decay curve and can be expressed as

$$\dot{Q} = V \frac{T_{ntp}}{T p_{ntp}} \frac{dp}{dt} \quad (20)$$

where V is the combined volume of the vessel and the sample line, T is the temperature of the gas in the volume and T_{ntp} and p_{ntp} are normal temperature and pressure. This method was used to measure the leak rates of Thermiculite 866, either uncoated or glass-coated.

5.2.2 Stack testing

Hybrid seals were tested in a single-cell stack in order to observe material interactions between seal materials and other stack components during operation. The stack used a cross-flow configuration. Its metallic components were made of Crofer 22 APU (ThyssenKrupp). The anode-supported cell was provided by Elcogen AS and its dimension was 100 mm x 100 mm. Hybrid seals were used for all seals located between Crofer 22 APU plates and are made with Thermiculite 866 between two glass tapes of 220 μ m green thickness. The glass used is a commercial product from Schott (GM31107), which belongs to the system MO (M = Mg, Ca)-Al₂O₃-BaO-SiO₂-B₂O₃ [130]. The Thermiculite 866 is composed in nearly equal amount of vermiculite and steatite, the compositions of which are [(K, Mg, Fe)₃(Si,Al)₄O₁₀(OH)₂] and [(Mg₃Si₄(OH)₂] respectively. The seal between the cell electrolyte and Crofer 22 APU plate was made of a glass tape without Thermiculite 866. Forty kilograms of weight was added on the stack, which corresponds to a compressive stress on the seal of ca. 0.1 MPa, assuming all the weight was carried by the seals and not by the cell.

Dry hydrogen and dry air (ca. 0.1%-vol water) were used as fuel and oxidant. Pure hydrogen exposes the seals to a worst-case condition as the leak rate through the hybrid seal increases with the concentration of hydrogen as discussed in Section 5.3. The stack was operated at 700 °C for 1800 h. The average current density was 0.2 A cm⁻² and fuel utilisation and air utilisation were both 18%. The hydrogen cross leak value was calculated from the relative humidity at the cathode outlet according to the following equation.

$$\dot{Q}_{H_2}^{cross} = X_{H_2O}^{C,out} \left(\dot{Q}_{Air}^{C,in} - \frac{I}{4F} \frac{RT_{ntp}}{p_{ntp}} \right) \quad (21)$$

where $X_{H_2O}^{C,out}$ is the steam molar fraction at the cathode outlet, $\dot{Q}_{Air}^{C,in}$ is the cathode air inlet flow, I is the current drawn from the stack, and F is the Faradic constant. These calculations are based on the assumption that the different leak rates are small compared to the cathode air flow.

After the test, the stack was mounted in epoxy resin and a cross-section sample was extracted near the air outlet for SEM and EDS analysis.

5.3 Results and discussion

The leak rate of seals made of Thermiculite 866 and glass-coated Thermiculite 866 were investigated in order to assess the improvement brought by the addition of a compliant glass layer between the Thermiculite 866 and the adjacent sealing surfaces. The leak rates of seals were studied as a function of the pressure difference across the seal and gas composition. In addition, a stack using a hybrid seal was assembled, tested and post-experimental microscopy analysis was conducted to study possible material interactions between seal materials and other stack components.

The leak rates as a function of pressure at compression stress of 0.1 and 0.4 MPa are detailed in Figure 24. The Thermiculite 866 was coated by wet spraying and the glass coating after heat treatment was about 10 μm . It can be seen that coating the Thermiculite 866 with glass decreases the leak rate, especially at low compressive stress. At low compressive stress and with a pressure difference of 20 mbar, the leak rate of the coated Thermiculite 866 is about $0.4 \text{ ml (m min)}^{-1}$, which is a reduction of about 85% compared to the uncoated one ($2.7 \text{ ml (m min)}^{-1}$). The allowable leak rate in an SOFC stack is specific to the design of the stack and its operation conditions. However, it is common sense to strive to develop a seal with the lowest leak rate at low compression stress to limit the fuel loss that limits the SOFC efficiency, and to decrease the risk of local oxidation of the nickel due to air leakage to the anode side. The results presented here are coherent with findings in the literature, although direct comparisons are difficult due to different conditions used. Chou et al. reported leak rates below $1 \text{ ml (m min)}^{-1}$ using hybrid seals made of mica paper coated with glass at compressive stresses of 0.04–0.7 MPa [118,121,131].

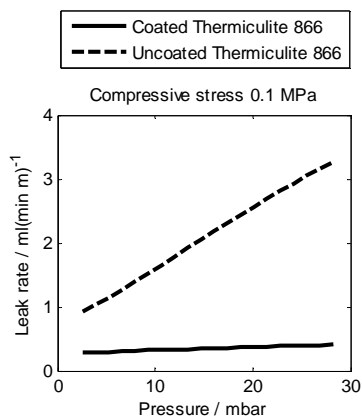


Figure 24. Leak rates of coated and uncoated Thermiculite 866 at compressive stress of 0.1 MPa in 50%-vol H₂ in N₂.

Figure 25 presents the leak rates as a function of pressure for coated and uncoated Thermiculite 866 with different hydrogen fractions. It can be seen that the uncoated Thermiculite 866 exhibits a leak rate which depends on the pressure difference and the gas composition. Conversely, the leak rate of the coated Thermiculite 866 depends only on the hydrogen concentration and is independent of the pressure difference. These results suggest that glass coating effectively blocks the direct interfacial leak paths and the remaining observed leak rate is due to concentration-driven diffusion rather than pressure-driven advection.

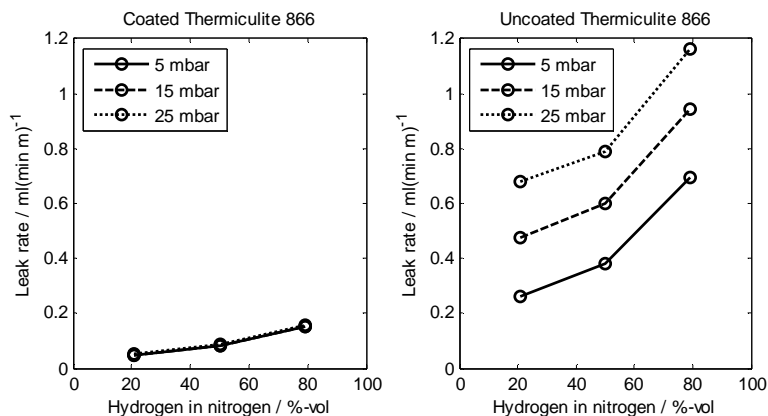


Figure 25. Leak rates of coated (left) and uncoated (right) Thermiculite 866 at different pressure differences as a function of hydrogen concentration. Compressive stress is 0.4 MPa.

A cross-section of a single-cell stack operated for 1800 h was investigated by SEM and EDS in order to investigate seal microstructure and possible material interactions. Figure 26 illustrates a cross-section of two hybrid seals from a single-cell stack. It can be observed that the glass has effectively covered the Thermiculite 866 and adapted to the thickness variations. For example, the dye-cutting process used to cut the seal to shape can form cutting burrs near the edges of the seal. This effect is particularly marked in the upper seal, where the glass coating has accommodated a gap varying from 15 to 150 μm . Some porosity can be seen in the glass where it is at its thickest (at the “150 μm ” annotation in Figure 26). However, the pores are closed and do not form a continuous leak path. Additionally, the gap clearances between the Crofer 22 APU plates are 710 and 580 μm at the location of measurement, and this difference did not seem to affect the quality of the seal at this location. This illustrates the benefits of using hybrid seals over purely compressible seals. In short, similar hybrid seals were able to effectively seal gaps of 710 and 576 μm and the glass layer was able to accommodate up to 140 μm of thickness variation in the Thermiculite 866. Compressive seals would have needed much higher compression stress in order to effectively accommodate the different gap clearance and to flatten the cutting burrs. Variations in gap clearance can be caused by the variation of thickness of the stack components (cells, gaskets, interconnects). This variation can be minimised by tight manufacturing tolerance, but this comes at higher costs. Therefore, it is highly advantageous to have a sealing solution that can accommodate the geometric variation in a stack.

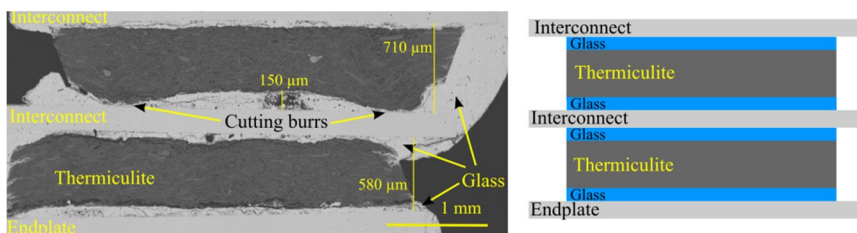


Figure 26. SEM-BSE cross-section of two hybrid seals. The seals are composed of a Thermiculite 866 core between two glass layers.

At nominal condition, the hydrogen cross leak value corresponded to a loss of 0.9% of the inlet hydrogen flow, which is a promising result for the first short-stack using this type of hybrid seal. Moreover, the hydrogen cross leak value remained constant during the 1800 h of the test as illustrated in Figure 27, showing that the performance of the seal did not degrade over time.

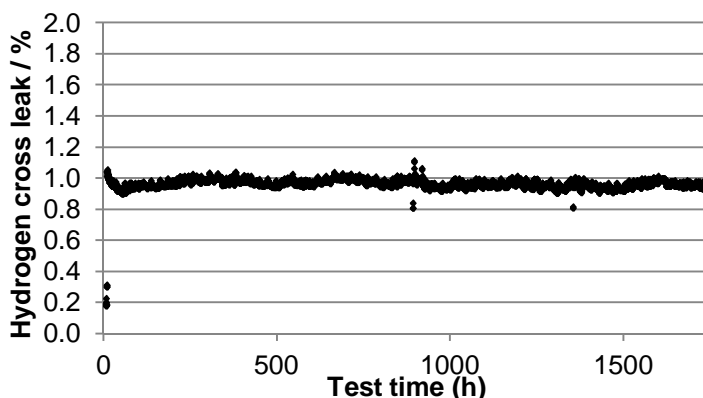


Figure 27. Hydrogen cross leak expressed as a percentage of the hydrogen fuel inlet flow.

The Crofer/glass and glass/Thermiculite 866 interfaces are shown in Figure 28. The location corresponds to the middle of a seal section, therefore the exposure to gas is limited to the leak through the seals. The oxide layer is found to be less than 1 μm, which corresponds to the oxide layer thickness of the interconnect far from the seal location. It appears that the glass has not affected the oxidation of the steel and therefore material interactions are limited at this interface. Additionally, there is no visible interaction between the glass and Thermiculite 866.

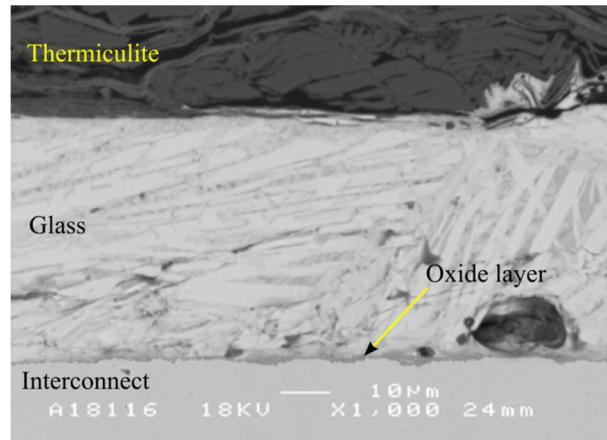


Figure 28. SEM-BSE cross-section of Crofer/glass and glass/Thermiculite 866 interfaces.

Four Crofer/glass/air interfaces are illustrated in Figure 29 and Figure 30. Figure 29 (a) and (b) depicts the upper and lower corners of the same seal exposed to the same cathode atmosphere. Despite the fact that they are exposed to the same conditions, their oxidation behaviour is very different. The upper seal does not exhibit any significant corrosion, whereas an oxidation layer of 20 μm in thickness has developed where the seal glass layer ends. The oxidation layer extends about 200 μm from the three-phase boundary. The composition of the oxidation layer has been investigated by EDS (Figure 29 (d)) and shows that the oxide layer is divided into an inner layer composed mainly of chromium oxide and a top layer composed of iron oxide. This corresponds to a break-away oxidation, i.e. when the chromium oxide can no longer protect the steel from rapid oxidation.

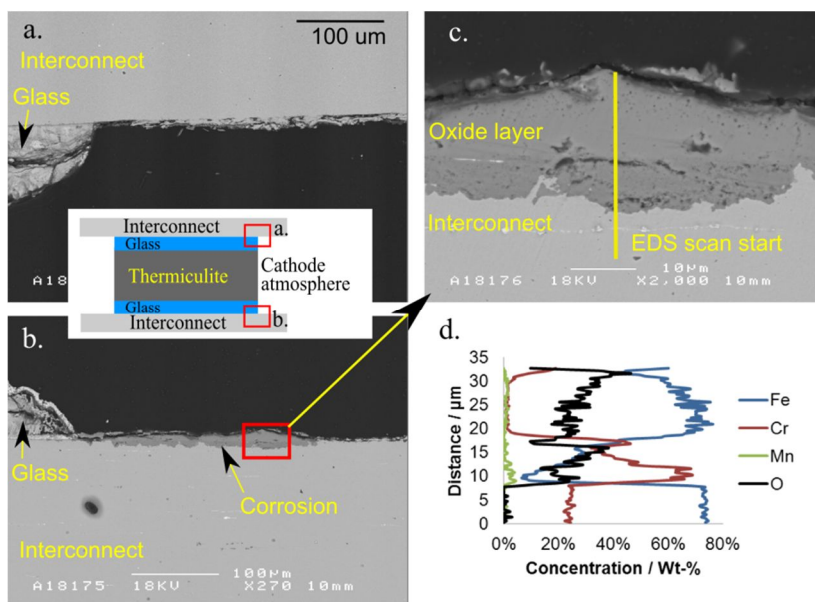


Figure 29. SEM-BSE cross-sections of two Crofer/glass/air interfaces (a and b) that are both exposed to cathode atmosphere. Magnified view of cross-section (c).

Similarly, Figure 30 depicts the three-phase interfaces of two different seals but which are exposed to the same air exhaust atmosphere from the air manifold. Also in this case, one interface (Figure 30 (a)) exhibits no significant oxidation, whereas a 20 μm-thick oxidation layer can be seen on the steel at the three-phase interface. Accelerated oxidation was also found further in the air manifold towards the stack air outlet. The oxide layer was thickest 5 mm away from the air manifold seals, where its thickness reached 120 μm (picture not shown). However, corrosion in the manifold of the thick endplate is not critical for stack performance.

There can be different causes for accelerated oxidation of the interconnect stainless steel. Chromium evaporation is enhanced in the presence of water vapour [91]. The water vapour concentration can be locally higher due to a hydrogen leak into the air atmosphere. However, this is not the case here, because there is air on both sides of the seals where accelerated oxidation was found. The heavy oxidation that was found deep in the manifold could be attributed to the presence of lubricant from machining. The endplates were lubricated during machining and were subsequently heat-treated (800 °C for 12 hours), polished and only then cleaned in a laboratory dishwasher and wiped with ethanol-impregnated tissues. However, it is difficult to remove lubricant or residue from burned lubricant from the narrow manifolds. This hypothesis is supported by the fact that the heaviest oxidation was found deep in the manifold, away from the seals. Lastly, the corrosion could be attributed to the transport of elements from the glass or the Thermiculite 866 to the stainless steel, where they could promote rapid corrosion.

However, if material interaction was the corrosion mechanism, one would expect it to happen systematically like in [126,127], which is not the case here.

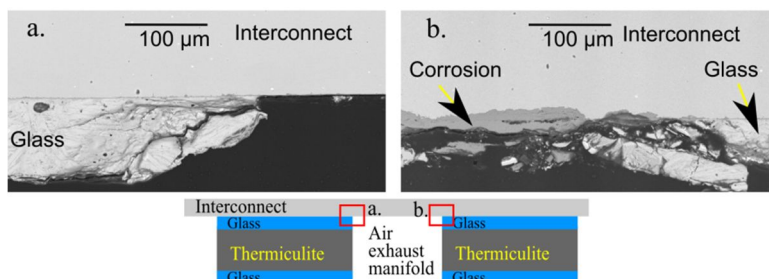


Figure 30. SEM-BSE cross-sections of two Crofer/glass/air interfaces (a and b) that are both exposed to the atmosphere of the air exhaust manifold.

Bram et al. also found accelerated oxidation in their work on material interaction between Thermiculite 866 and Crofer 22 APU (no glass used) [127]. They exposed their sample in ambient air at 600 °C for 400 h, which resulted in a very thick oxide layer (80–100 µm) that extended more than one mm away from the Thermiculite 866. They attributed the corrosion to an increase of water vapour content due to the dehydration of vermiculite and the decomposition of steatite. Wiener et al. also conducted research on the material interaction between Crofer 22 APU and Thermiculite 866 [126]. They exposed their Thermiculite material to 800 °C for 400 h in ambient air and also found accelerated oxidation. Their oxide layer was about 20 µm in thickness near the seal material. They explained the oxidation behaviour by the transport of magnesium from the steatite contained in the Thermiculite 866.

The most likely reason for the observed accelerated corrosion in the tested stack was attributed to the contamination from lubricant that was not properly removed during stack assembly. However, material interaction between the glass and the Thermiculite 866 cannot be ruled out. The main risks associated with oxidation on the interconnect in the vicinity of the seals is either the formation of porous oxidation product all the way through the 0.2 mm interconnect or that the oxidation product forms a conductive bridge between two interconnects, resulting in short-circuiting. However, in our case the extent of corrosion is rather limited after 1800 h. Corrosion was only found at the three-phase interface between glass, steel and air, which is consistent with the results of several previous study [62,125-127]. Therefore, the author recommends that the three-phase interface should always be included in material interaction studies between seals and interconnects.

The last interfaces investigated were the Crofer/glass/humid hydrogen interface, illustrated in Figure 31, and the glass/YSZ-electrolyte interface in Figure 32. The Crofer 22 APU oxide layer is below 1 µm next to the glass seal and no visible interaction is visible between the glass and the electrolyte material. In short, no

accelerated oxidation could be observed at the three-phase interface Crofer/glass/humid hydrogen and between the glass and the electrolyte materials.

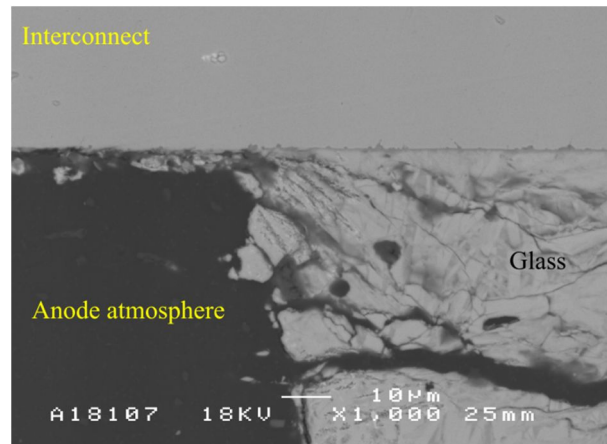


Figure 31. SEM-BSE cross-section at the Crofer/glass/humid hydrogen interface. The visible glass is part of the cell seal which is composed of glass without any Thermiculite 866.

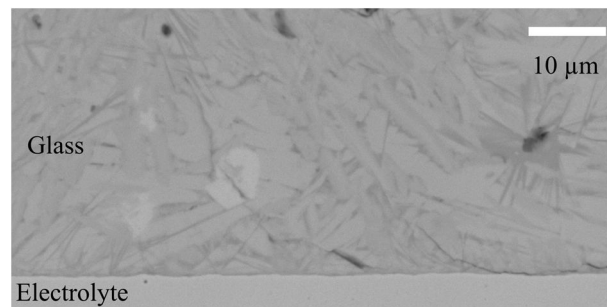


Figure 32. SEM-BSE cross-section at the interface between glass and electrolyte.

6. Summary and conclusions

SOFC systems are expected to play an important role in the power generation sector due to their advantages in terms of high efficiency, fuel flexibility, modularity and very low emissions. However, their high cost remains a burden delaying their market entry. In order to drive their cost down, their durability must be improved and system complexity needs to be reduced. The work presented in this dissertation addresses these two challenges by the prevention of chromium poisoning of the cathode, by demonstrating the possibility to decrease the complexity of the fuel processing subsystem and by the development of a performant and durable type of seal.

Chromium poisoning of the cathode causes a degradation of its performance and it is seen as a major issue limiting the durability of SOFC. A protective coating solution was developed to limit chromium transport from the stainless steel interconnect to the cathode and by the development of a method to quantify the amount of chromium species originating from BoP components.

Protective MnCo_2O_4 and $\text{MnCo}_{1.8}\text{Fe}_{0.2}\text{O}_4$ coatings were manufactured on SOFC interconnect steel by High Velocity Oxy Fuel spraying coating. The coating effectively reduced the oxidation rate of the steel substrate in a high-temperature exposure test. The ASR was measured from coated samples and showed that the ASR did not exhibit degradation during the 1000 h test at 700 °C. The suitability of the coating solution was further assessed by performing a post-experimental analysis of a single-cell stack with a coated interconnect that was operated for 6000 h. It confirmed that the coating effectively reduced the oxidation of the interconnect and that the coating did not exhibit cracks or open porosity. Additionally, chromium could not be detected in the coating, suggesting that the chromium diffusion through the coating was sufficiently low. A low concentration of chromium was detected in the SOFC cathode. However, the uncoated steel manifold and piping upstream of the stack are also known to be a source of volatile chromium and are likely to be the source of the chromium found in the cathode. Overall, the coating developed is promising in terms of improving the durability of SOFC stacks by preventing interconnect oxidation and chromium poisoning of the cathode. The suitability of the coating should be further assessed in accelerated ageing stack tests with humidified air because humidity is known to increase the evaporation rate of chromium from stainless steel [91]. Additionally, electrochemical imped-

ance spectroscopy should be performed during future stack tests to follow the different contributions to the ASR behaviour during ageing. Obviously, adding any type of coating increases the cost associated with the SOFC stack, but coatings that effectively reduces oxidation of the steel allow the use of cheaper grade steel such as AISI441 (EN 1.4509) [132]. Using a cheaper grade of steel is likely to offset the cost associated with the coating to some extent.

The findings of Publication I suggested that the stainless steel components upstream of the cathode are a potential source of volatile chromium. To gain insight into this contamination source, a method for quantifying chromium evaporation from BoP component was developed and evaluated on a stainless steel pipe in Publication II. The principle of the method is to collect volatile chromium species by sampling hot air directly from a BoP component through a denuder tube coated with sodium carbonate. The chromium species react with the sodium carbonate coating, which is then dissolved and its chromium content analysed by ICP-MS.

The developed method proved to be an effective tool because its results were found to be coherent with thermodynamics data from the literature and it yielded repeatable results. These results confirmed that stainless steel BoP components are a source of volatile chromium that can poison the cathode of SOFC. Therefore, future research should address the issue of reducing chromium transport from the hot stainless steel BoP component to the cathode. The experimental set-up is designed in a way that enables its implementation after a BoP component, such as a heat exchanger or at various places within an SOFC system. This makes the assessment of local chromium concentration possible at the stack air inlet or outlet. Therefore, the method enables identification of the major chromium sources of the system that can contaminate the SOFC cathode and is a tool for assessing the effectiveness of solutions such as protective coatings, surface treatments, chromium trap, and material selection to mitigate chromium transport from BoP components to the cathode.

Two simplifications of the fuel subsystem are proposed in this dissertation. The first is to eliminate the external water supply during SOFC operation. A steam supply is needed for the steam reforming reaction taking place in the fuel processing subsystem. The steam can either be supplied externally, which requires a water inlet and an evaporator or it can be supplied by recycling the steam-rich anode off-gas, which simplifies the system. Recycling the anode off-gas has been extensively studied because it can also improve electrical efficiency of SOFC system, but most of the publications focus on simulation work. However, using anode off-gas recycling increases the risk of carbon formation in the pre-reformer at low recycling ratios and its effect on the activity of a precious metal catalyst has not been published in the literature before Publication III. In Publication III, a commercial precious metal catalyst was tested in steam reforming conditions and in simulated anode off-gas recycling (AOGR) conditions. It was found that the catalyst is more active in AOGR mode for the evaluated conditions, therefore the pre-reformer dimension can be reduced if AOGR is used in a system instead of supplying the water externally. Additionally, long-term tests demonstrated that the tested catalyst did not form carbon to an extent that would threaten SOFC system

operation in AOGR conditions. The results of this study demonstrated that the tested pre-reformer can be used in a system with an AOGR loop. Based on these results, an AOGR loop was successfully implemented in a 10 kW demonstration SOFC system. The system relied solely on AOGR to provide the necessary steam for natural gas reforming and no external water was used at nominal conditions. In the future, additional kinetics analysis could be performed to understand the observed difference in catalyst activity in steam reforming and AOGR conditions. The experiments presented in this dissertation were using grid natural gas and in Finland, its higher hydrocarbon content (ethane and propane) is particularly low. Therefore, supplementary experiments could be conducted with natural gas containing more higher hydrocarbon in order to investigate the conversion of ethane and propane by the developed pre-reformer.

The second system simplification proposed is to heat up an SOFC system by using the pre-reformer to generate hydrogen-containing protective gas. The protective gas is needed to prevent the nickel of the anode from reoxidising, which is detrimental for the SOFC stack durability. The reducing protective gas is often provided from cylinders of premixed hydrogen and nitrogen. However, the premixed gas cylinders increase the system size and their replacement adds up to the maintenance cost of the system, therefore it would be beneficial to generate the hydrogen-containing gas with the pre-reformer during heat-up.

The activity of the pre-reformer catalyst at temperatures as low as 200 °C was tested for the steam reforming reaction. It was found that the catalyst had measurable activity below 250 °C, but if oxygen originating from leakage was present, the reaction was inhibited below ca. 400 °C. However, the oxygen could be consumed by the addition of hydrogen at temperatures as low as 200 °C. These results were used to develop a heat-up procedure for a 10 kW SOFC system including a pre-reformer and an AOGR loop. The pre-reformer was used for two purposes: firstly, to remove molecular oxygen from the fuel side by the catalytic combustion of a small feed of hydrogen and secondly, to provide a reducing atmosphere to the SOFC anode by reforming a small fraction of the natural gas feed. The difference of the cell voltage before and after the heat-up procedure did not reveal any performance degradation. Therefore, it was considered that the heat-up procedure fulfilled its requirements and it allows for a reduction of the system size and its complexity by making the premixed gas cylinders unnecessary for heat-up. At the time of writing, no experimental work describing the heat-up of a planar SOFC system with AOGR had been published previously.

The results showed that a steam generator and a water feed are not needed during operation, i.e. when current is drawn from the stack. However, the heat-up procedure presented in this work relies on a steam feed for the steam reforming of the natural gas. Therefore, future research should focus on the development of a procedure to generate the hydrogen-containing protective gas without the need for a steam feed. For this purpose, the use of catalytic partial oxidation of natural gas is suggested.

A method for producing hybrid seals consisting of a compressible core coated with compliant glass was presented in Publication V. The aim of this development was to achieve low leak rate at low compression stresses. The novelty of the hybrid seals investigated in this dissertation is in the core material chosen that contains a steatite filler between vermiculite platelets, which results in improved gas tightness and superior compressibility. The developed solution exhibited a leak rate of about $0.4 \text{ ml (min m)}^{-1}$ at 20 mbar pressure difference using a compressive stress of 0.1 MPa. This is an 85% reduction compared to uncoated Thermiculite 866. The leak rate performance of the developed seal was considered very promising. The coated Thermiculite 866 could be handled in exactly the same way as uncoated gasket, thus enabling a simple stack assembling method. Using the developed hybrid seals instead of compressive seals allows a significant reduction in the compression need on the stack, which enables the simplification of the stack compression system.

While the leak rate performance of the developed hybrid seal makes it an attractive sealing solution, the durability of the SOFC stack requires limited material interactions between the materials of the hybrid seals and other stack components during operation. For this purpose, a post-experimental analysis was performed on a stack using hybrid seals after 1800 h of operation (Publication VI). Different locations inside the stack were investigated. No corrosion could be found at the two-phase interfaces such as Crofer/glass, glass/electrolyte and glass/Thermiculite 866. The three-phase interfaces between Crofer/glass/hydrogen exhibited no corrosion, whereas interfaces corresponding to Crofer/glass/air exhibited some non-systematic corrosion. The possible reasons for the corrosion discovered were discussed and the most likely was the contamination from lubricant that was not properly removed during stack assembly.

The developed hybrid seal can be used together with the coated interconnect used in Publication I. However the coating should only be applied where it will be exposed to oxidative atmosphere (cathode side). The reason for that is that the reductive atmosphere of the anode is likely to reduce the coating to its metallic form and to make it porous.

Further research should focus on validating the hypothesis concerning the corrosion found near the hybrid seals in air atmosphere. Additionally, the long-term suitability of the hybrid seal materials should be investigated either in longer-term stack tests or by using accelerated ageing conditions such as increasing the air humidity content to 1...3%. Moreover, tests should be performed to compare the durability of glass and hybrid seals after numerous thermal cycles as it is known that thermal cycling is more critical towards durability than steady conditions.

The performance of the developed seal are very promising in terms of leak rate and material compatibility and the results presented in this section led to the commercialisation of the developed seal by Flexitallic under the brand "Thermiculite 866 LS", which is a glass-coated version of the Thermiculite 866 product [1,133].

SOFCs have demonstrated very good performance in terms of electrical efficiency, which makes them a promising technology for the power generation sector. At the same time, SOFCs need to show rapid technological progress towards commercialization in order to sustain investment in research and development effort. The main obstacle is their high cost: SOFC stacks are expensive and their lifetime is limited due to degradation. Additionally, system BoP components are costly, because many of these components are not found off-the-shelf or produced in small series. There is no doubt that costs will be decreased by economies of scale when SOFCs are mass produced. However, scientific research has a key role to play in reducing the cost of SOFCs. Important topics are cost-effective solutions to improve SOFC durability. In the field of interconnect, coating methods suitable for mass production should be investigated. Additionally, the protective coating should enable using standard ferritic stainless steel grades that are much cheaper than alloys specifically design for SOFCs. An example of such progress is the roll-to-roll coating method of Sandvik [134]. On the system level, BoP components development include the integration of the catalytic reactor and the heat exchanger. For example, Lee et al. presented the development of a heat exchanger, with channels catalytically active for steam reforming and others for afterburner of the anode off-gas [135]. Other simplifications concern the instrumentation of the system. For example, stack temperature is difficult to measure. However, the maximum stack temperature could be estimated by accurate data-based models, making direct measurement unnecessary [136].

References

- [1] Flexitallic Ltd., Thermiculite ® 866 / 866 LS, 2014, Last accessed 08.01.2015 2015, <http://www.flexitallicsofc.com/downloads/thermiculite866.pdf>.
- [2] Intergovernmental panel on climate change - IPCC, Fifth Assessment Report (AR5), Cambridge University Press, Cambridge, United Kingdom and New York, NY, USA, 2014.
- [3] European Environment Agency, Annual European Union Greenhouse Gas Inventory 1990–2012 and Inventory Report 2014, Publications Office of the European Union, Luxembourg, 2014.
- [4] European Environment Agency, EEA Greenhouse gas - Data viewer, 2015, Last accessed 16.01 2015, <http://www.eea.europa.eu/data-and-maps/data/data-viewers/greenhouse-gases-viewer>.
- [5] P. Capros, A. De Vita, N. Tasios, D. Papadopoulos, P. Siskos, E. Apostolaki, M. Zampara, L. Paroussos, K. Fragiadakis, N. Kouvaritakis, L. Höglund-Isaksson, W. Winiwarter, P. Purohit, H. Böttcher, S. Frank, P. Havlik, M. Gusti, H.P. Witzke, EU Energy, Transport and GHG Emissions, Trends to 2050. Publications office of the European Union, Luxembourg, 2013.
- [6] L. Chick, M. Weimar, G. Whyatt, M. Powell, The Case for Natural Gas Fueled Solid Oxide Fuel Cell Power Systems for Distributed Generation, Fuel Cells. 15.1 (2015) 49-60.
- [7] S.C. Singhal, Solid oxide fuel cells for stationary, mobile, and military applications, Solid State Ionics. 152-153 (2002) 405-410.
- [8] R. Payne, J. Love, M. Kah, Generating Electricity at 60% Electrical Efficiency from 1-2 kWe SOFC Products, ECS Trans. 25 (2009) 231-239.
- [9] K. Sasaki, K. Watanabe, K. Shiosaki, K. Susuki, Y. Teraoka, Multi-fuel capability of solid oxide fuel cells, J Electroceram. 13 (2004) 669-675.
- [10] K. Eguchi, H. Kojo, T. Takeguchi, R. Kikuchi, K. Sasaki, Fuel flexibility in power generation by solid oxide fuel cells, Solid State Ionics. 152-153 (2002) 411-416.
- [11] G. Gahleitner, Hydrogen from renewable electricity: An international review of power-to-gas pilot plants for stationary applications, Int J Hydrogen Energy. 38 (2013) 2039-2061.
- [12] E4tech, The Fuel Cell Industry Review 2014, Lausanne, Switzerland, 2014.

- [13] Fuel cell and hydrogen joint undertaking (FCH JU), Multi Annual Implementation Plan 2008-2013. 2011.
- [14] H. Yokokawa, H. Tu, B. Iwanschitz, A. Mai, Fundamental mechanisms limiting solid oxide fuel cell durability, *J. Power Sources*. 182 (2008) 400-412.
- [15] R.M. Ormerod, Solid oxide fuel cells, *Chem. Soc. Rev.* 32 (2003) 17-28.
- [16] S.J. Skinner, Recent advances in Perovskite-type materials for solid oxide fuel cell cathodes, *International Journal of Inorganic Materials*. 3 (2001) 113-121.
- [17] D.J.L. Brett, A. Atkinson, N.P. Brandon, S.J. Skinner, Intermediate temperature solid oxide fuel cells, *Chem. Soc. Rev.* 37 (2008) 1568-1578.
- [18] E. Konyshova, H. Penkalla, E. Wessel, J. Mertens, U. Seeling, L. Singheiser, K. Hilpert, Chromium poisoning of perovskite cathodes by the ODS alloy Cr5Fe1 Y2 O3 and the high chromium ferritic steel Crofer22APU, *J. Electrochem. Soc.* 153 (2006) A765-A773.
- [19] K. Hilpert, D. Das, M. Miller, D.H. Peck, R. Weiß, Chromium vapor species over solid oxide fuel cell interconnect materials and their potential for degradation processes, *J. Electrochem. Soc.* 143 (1996) 3642-3647.
- [20] J. Wu, X. Liu, Recent Development of SOFC Metallic Interconnect, *J. Mater. Sci. Technol.* 26 (2010) 293-305.
- [21] J.W. Fergus, Metallic interconnects for solid oxide fuel cells, *Materials Science and Engineering A*. 397 (2005) 271-283.
- [22] W.Z. Zhu, S.C. Deevi, Development of interconnect materials for solid oxide fuel cells, *Mater. Sci. Eng. A*. 348 (2003) 227-243.
- [23] N. Shaigan, W. Qu, D.G. Ivey, W. Chen, A review of recent progress in coatings, surface modifications and alloy developments for solid oxide fuel cell ferritic stainless steel interconnects, *J. Power Sources*. 195 (2010) 1529-1542.
- [24] Z. Yang, K.S. Weil, D.M. Paxton, J.W. Stevenson, Selection and Evaluation of Heat-Resistant Alloys for SOFC Interconnect Applications, *J. Electrochem. Soc.* 150 (2003).
- [25] P.D. Jablonski, C.J. Cowen, J.S. Sears, Exploration of alloy 441 chemistry for solid oxide fuel cell interconnect application, *J. Power Sources*. 195 (2010) 813-820.
- [26] Y. Chou, J.W. Stevenson, J. Choi, Long-term evaluation of solid oxide fuel cell candidate materials in a 3-cell generic stack test fixture, part III: Stability and mi-

crostructure of Ce-(Mn,Co)-spinel coating, AISI441 interconnect, alumina coating, cathode and anode, J. Power Sources. 257 (2014) 444-453.

[27] Z. Yang, G.-G. Xia, C.-M. Wang, Z. Nie, J. Templeton, J.W. Stevenson, P. Singh, Investigation of iron-chromium-niobium-titanium ferritic stainless steel for solid oxide fuel cell interconnect applications, J. Power Sources. 183 (2008) 660-667.

[28] M.W. Lundberg, R. Berger, J. Westlinder, N. Folkesson, H. Holmberg, Novel multilayered PVD-coating in a roll to roll mass production process, ECS Transactions. 57 (2013) 2203-2208.

[29] J.W. Stevenson, Z.G. Yang, G.G. Xia, Z. Nie, J.D. Templeton, Long-term oxidation behavior of spinel-coated ferritic stainless steel for solid oxide fuel cell interconnect applications, J. Power Sources. 231 (2013) 256-263.

[30] J.W. Fergus, Sealants for solid oxide fuel cells, J. Power Sources. 147 (2005) 46-57.

[31] K. Weil, The state-of-the-art in sealing technology for solid oxide fuel cells, JOM. 58 (2006) 37-44.

[32] Z. Wullemmin, N. Autissier, M. Nakajo, M. Luong, J. Van Herle, D. Favrat, Modeling and study of the influence of sealing on a solid oxide fuel cell, J. Fuel Cell Sci. Technol. 5 (2008).

[33] Y. Chou, J.W. Stevenson, R.N. Gow, Novel alkaline earth silicate sealing glass for SOFC: Part II. Sealing and interfacial microstructure, J. Power Sources. 170 (2007) 395-400.

[34] A. Shyam, R. Trejo, D. McClurg, A. Ladouceur, M. Kirkham, X. Song, J. Howe, E. Lara-Curzio, Microstructural evolution in two alkali multicomponent silicate glasses as a result of long-term exposure to solid oxide fuel cell environments, J. Mater. Sci. 48 (2013) 5880-5898.

[35] M. Rautanen, O. Himanen, V. Saarinen, J. Kiviaho, Compression properties and leakage tests of mica-based seals for SOFC stacks, Fuel Cells. 9 (2009) 753-759.

[36] S.P. Simner, J.W. Stevenson, Compressive mica seals for SOFC applications, J. Power Sources. 102 (2001) 310-316.

[37] Y.-S. Chou, J.W. Stevenson, L.A. Chick, Ultra-low leak rate of hybrid compressive mica seals for solid oxide fuel cells, J. Power Sources. 112 (2002) 130-136.

- [38] Y.-S. Chou, J.W. Stevenson, L.A. Chick, Novel compressive mica seals with metallic interlayers for solid oxide fuel cell applications, *J Am Ceram Soc.* 86 (2003) 1003-1007.
- [39] D. Mogensen, J.-D. Grunwaldt, P.V. Hendriksen, K. Dam-Johansen, J.U. Nielsen, Internal steam reforming in solid oxide fuel cells: Status and opportunities of kinetic studies and their impact on modelling, *J. Power Sources.* 196 (2011) 25-38.
- [40] Y. Yi, A.D. Rao, J. Brouwer, G.S. Samuelsen, Fuel flexibility study of an integrated 25 kW SOFC reformer system, *J. Power Sources.* 144 (2005) 67-76.
- [41] S.L. Douvartzides, F.A. Coutelieres, A.K. Demin, P.E. Tsiakaras, Fuel options for solid oxide fuel cells: A thermodynamic analysis, *AIChE J.* 49 (2003) 248-257.
- [42] R.-U. Dietrich, J. Oelze, A. Lindermeir, C. Spieker, C. Spitta, M. Steffen, Power generation from biogas using SOFC - Results for a 1kWe demonstration unit, *Fuel Cells.* 14 (2014) 239-250.
- [43] M. Halinen, M. Rautanen, J. Saarinen, J. Pennanen, A. Pohjoranta, J. Kiviaho, M. Pastula, B. Nuttall, C. Rankin, B. Borglum, Performance of a 10 kW SOFC Demonstration Unit, *ECS Transactions.* 35 (2011) 113-120.
- [44] K. Ahmed, J. Gamman, K. Föger, Demonstration of LPG-fueled solid oxide fuel cell systems, *Solid State Ionics.* 152-153 (2002) 485-492.
- [45] Y. Du, D. Cui, K. Reifsnider, Characterization of propane-fueled SOFC portable power systems, *ECS Transactions.* 35 (2011) 167-178.
- [46] P. Leone, A. Lanzini, G.A. Ortigoza-Villalba, R. Borchellini, Operation of a solid oxide fuel cell under direct internal reforming of liquid fuels, *Chem. Eng. J.* 191 (2012) 349-355.
- [47] M. Rautanen, M. Halinen, M. Noponen, K. Koskela, H. Vesala, J. Kiviaho, Experimental study of an SOFC stack operated with autothermally reformed diesel fuel, *Fuel Cells.* 13 (2013) 304-308.
- [48] D. Shekhawat, D.A. Berry, J.J. Spivey, *Fuel Cells: Technologies for Fuel Processing*, Elsevier Ltd., Oxford, UK, 2011.
- [49] Union Gas, Chemical Composition of Natural Gas, 2015, Last accessed 01.22 2015, <http://www.uniongas.com/about-us/about-natural-gas/Chemical-Composition-of-Natural-Gas>.
- [50] Energinet.dk, Vis gaskvalitet, 2013, Last accessed 01.22 2015, <http://energinet.dk/DA/GAS/Gasdata-og-kvalitet/Gaskvalitet/Sider/Vis-gaskvalitet.aspx?Visning=aarsgennemsnit>.

- [51] Gasum Oy, Natural Gas Composition Yearly Report, 2012.
- [52] R. Peters, R. Dahl, U. Klüttgen, C. Palm, D. Stolten, Internal reforming of methane in solid oxide fuel cell systems, *J. Power Sources*. 106 (2002) 238-244.
- [53] S. McIntosh, R.J. Gorte, Direct hydrocarbon solid oxide fuel cells, *Chem. Rev.* 104 (2004) 4845-4865.
- [54] J.N. Armor, The multiple roles for catalysis in the production of H₂, *Applied Catalysis A: General*. 176 (1999) 159-176.
- [55] L. Blum, E. Riensche, FUEL CELLS – SOLID OXIDE FUEL CELLS | Systems, in: J. Garche (Ed.), *Encyclopedia of Electrochemical Power Sources*, Elsevier, Amsterdam, 2009, pp. 99-119.
- [56] P. Gannon, R. Amendola, High-temperature, dual-atmosphere corrosion of solid-oxide fuel cell interconnects, *JOM*. 64 (2012) 1470-1476.
- [57] H. Tu, U. Stimming, Advances, aging mechanisms and lifetime in solid-oxide fuel cells, *J. Power Sources*. 127 (2004) 284-293.
- [58] M. Stanislawski, E. Wessel, K. Hilpert, T. Markus, L. Singheiser, Chromium vaporization from high-temperature alloys, *J. Electrochem. Soc.* 154 (2007).
- [59] M.C. Tucker, H. Kurokawa, C.P. Jacobson, L.C. De Jonghe, S.J. Visco, A fundamental study of chromium deposition on solid oxide fuel cell cathode materials, *J. Power Sources*. 160 (2006) 130-138.
- [60] J.A. Schuler, H. Yokokawa, C.F. Calderone, Q. Jeangros, Z. Wuillemin, A. Hessler-Wyser, J. Van Herle, Combined Cr and S poisoning in solid oxide fuel cell cathodes, *J. Power Sources*. 201 (2012) 112-120.
- [61] J.W. Fergus, Effect of cathode and electrolyte transport properties on chromium poisoning in solid oxide fuel cells, *Int J Hydrogen Energy*. 32 (2007) 3664-3671.
- [62] N.H. Menzler, P. Batfalsky, L. Blum, M. Bram, S.M. Groß, V.A.C. Haanappel, J. Malzbender, V. Shemet, R.W. Steinbrech, I. Vinke, Studies of material interaction after long-term stack operation, *Fuel Cells*. 7 (2007) 356-363.
- [63] Y. Larring, T. Norby, Spinel and perovskite functional layers between Plansee metallic interconnect (Cr-5 wt % Fe-1 wt % Y₂O₃) and ceramic (La_{0.85}Sr_{0.15})_{0.91}MnO₃ cathode materials for solid oxide fuel cells, *J. Electrochem. Soc.* 147 (2000) 3251-3256.
- [64] J.W. Fergus, Synergism in the design of interconnect alloy-coating combinations solid for oxide fuel cells, *Scr. Mater.* 65 (2011) 73-77.

- [65] X. Montero, N. Jordán, J. Pirón-Abellán, F. Tietz, D. Stöver, M. Cassir, I. Villarreal, Spinel and perovskite protection layers between crofer22APU and La 0.8Sr0.2FeO3 cathode materials for SOFC interconnects, *J. Electrochem. Soc.* 156 (2009) B188-B196.
- [66] J. Puranen, J. Lagerbom, L. Hyvärinen, M. Kylmälahti, O. Himanen, M. Pihlatie, J. Kiviaho, P. Vuoristo, The structure and properties of plasma sprayed iron oxide doped manganese cobalt oxide spinel coatings for SOFC metallic interconnectors, *J. Therm. Spray Technol.* 20 (2011) 154-159.
- [67] X. Chen, P.Y. Hou, C.P. Jacobson, S.J. Visco, L.C. De Jonghe, Protective coating on stainless steel interconnect for SOFCs: oxidation kinetics and electrical properties, *Solid State Ionics.* 176 (2005) 425-433.
- [68] Z. Yang, G. Xia, G.D. Maupin, J.W. Stevenson, Conductive protection layers on oxidation resistant alloys for SOFC interconnect applications, *Surf. Coat. Technol.* 201 (2006) 4476-4483.
- [69] A. Balland, P. Gannon, M. Deibert, S. Chevalier, G. Caboche, S. Fontana, Investigation of La2O3 and/or (Co,Mn)3O4 deposits on Crofer22APU for the SOFC interconnect application, *Surf. Coat. Technol.* 203 (2009) 3291-3296.
- [70] Y. Fang, C. Wu, X. Duan, S. Wang, Y. Chen, High-temperature oxidation process analysis of MnCo2O4 coating on Fe-21Cr alloy, *Int J Hydrogen Energy.* 36 (2011) 5611-5616.
- [71] J. Puranen, J. Lagerbom, L. Hyvärinen, T. Mäntylä, E. Levänen, M. Kylmälahti, P. Vuoristo, Formation and structure of plasma sprayed manganese-cobalt spinel coatings on preheated metallic interconnector plates, *Surf. Coat. Technol.* 205 (2010) 1029-1033.
- [72] K. Uusi-Esko, E.-L. Rautama, M. Laitinen, T. Sajavaara, M. Karppinen, Control of oxygen nonstoichiometry and magnetic property of MnCo 2O 4 thin films grown by atomic layer deposition, *Chem. Mater.* 22 (2010) 6297-6300.
- [73] L. Mikkelsen, M. Chen, P.V. Hendriksen, Å. Persson, N. Pryds, K. Rodrigo, Deposition of La0.8Sr0.2Cr0.97V0.03O3 and MnCr2O4 thin films on ferritic alloy for solid oxide fuel cell application, *Surf. Coat. Technol.* 202 (2007) 1262-1266.
- [74] M.J. Lewis, J.H. Zhu, A process to synthesize (Mn,Co) 3 O 4 spinel coatings for protecting SOFC interconnect alloys, *Electrochem. Solid-State Lett.* 14 (2011) B9-B12.
- [75] V.I. Gorokhovskiy, P.E. Gannon, M.C. Deibert, R.J. Smith, A. Kayani, M. Kopczyk, D. Vanvorous, Z. Yang, J.W. Stevenson, S. Visco, C. Jacobson, H. Kurokawa, S.W. Sofie, Deposition and evaluation of protective PVD coatings on ferritic stainless steel SOFC interconnects, *J. Electrochem. Soc.* 153 (2006) A1886-A1893.

- [76] L. Pawlowski, Thermal Spraying Techniques, The Science and Engineering of Thermal Spray Coatings, John Wiley & Sons, Ltd, 2008, pp. 67-113.
- [77] Z. Yang, G.-G. Xia, X.-H. Li, J.W. Stevenson, (Mn,Co)3O4 spinel coatings on ferritic stainless steels for SOFC interconnect applications, *Int J Hydrogen Energy*. 32 (2007) 3648-3654.
- [78] L. Mikkelsen, K. Neufeld, P.V. Hendriksen, Interface Resistance Between FeCr Interconnects and La_{0.85}Sr_{0.15}Mn₁O₃, *ECS Transactions*. 25 (2009) 1429.
- [79] Z. Yang, J.S. Hardy, M.S. Walker, G. Xia, S.P. Simner, J.W. Stevenson, Structure and conductivity of thermally grown scales on ferritic Fe-Cr-Mn steel for SOFC interconnect applications, *J. Electrochem. Soc.* 151 (2004) A1825-A1831.
- [80] J.A. Schuler, Z. Wullemmin, A. Hessler-Wyser, C. Comminges, N.Y. Steiner, J. Van Herle, Cr-poisoning in (La,Sr)(Co,Fe)O₃ cathodes after 10,000 h SOFC stack testing, *J. Power Sources*. 211 (2012) 177-183.
- [81] O. Thomann, M. Pihlatie, J.A. Schuler, O. Himanen, J. Kiviaho, Method for measuring chromium evaporation from SOFC balance-of-plant components, *Electrochem. Solid-State Lett.* 15 (2012) B35-B37.
- [82] Z. Wullemmin, N. Nakajima, A. Müllera, A. Schuler, S. Diethelm, J. Van herle, D. Favrat, Locally-resolved study of degradation in a SOFC, *ECS Trans.* 25 (2009) 457-466.
- [83] J.A. Schuler, C. Gehrig, Z. Wullemmin, A.J. Schuler, J. Wochele, C. Ludwig, A. Hessler-Wyser, J. Van Herle, Air side contamination in Solid Oxide Fuel Cell stack testing, *J. Power Sources*. 196 (2011) 7225-7231.
- [84] K. Gerdes, C. Johnson, Surface Scale Formation on Solid Oxide Fuel Cell Proximal Balance of Plant Components, *Journal of Fuel Cell Sci. & Tech.* vol. 6 (2009).
- [85] M. Stanislawski, E. Wessel, T. Markus, L. Singheiser, W.J. Quadackers, Chromium vaporization from alumina-forming and aluminized alloys, *Solid State Ionics*. 179 (2008) 2406-2415.
- [86] D. Chatterjee, S. Biswas, Development of chromium barrier coatings for solid oxide fuel cells, *Int J Hydrogen Energy*. 36 (2011) 4530-4539.
- [87] J.A. Schuler, A.J. Schuler, D. Penner, A. Hessler-Wyser, C. Ludwig, J. Van Herle, Mitigating Cr Contamination by Hot Air Filtering in Solid Oxide Fuel Cells, *Electrochemical and Solid-State Letters*. 14 (2011).

- [88] C. Key, J. Eziashi, J. Froitzheim, R. Amendola, R. Smith, P. Gannon, Methods to Quantify Reactive Chromium Vaporization from Solid Oxide Fuel Cell Interconnects, *Journal of The Electrochemical Society*. 161 (2014) C373-C381.
- [89] J. Froitzheim, H. Ravash, E. Larsson, L.G. Johansson, J.E. Svensson, Investigation of chromium volatilization from FeCr interconnects by a denuder technique, *J. Electrochem. Soc.* 157 (2010) B1295-B1300.
- [90] M. Casteel, P. Willson, T. Goren, P. O'Brien, D. Lewis, Novel Method for Measuring Chromia Evaporation from SOFC Interconnect Materials, *ECS Trans.* 25 (2009) 1423.
- [91] C. Gindorf, L. Singheiser, K. Hilpert, Vaporisation of chromia in humid air, *J. Phys. Chem. Solids*. 66 (2005) 384-387.
- [92] Outotec, HSC Chemistry, 6.12 (2007).
- [93] Sandvik, Sandvik 253MA, Last accessed 11/16 2011, <http://www.smt.sandvik.com/en/materials-center/material-datasheets/tube-and-pipe-seamless/sandvik-253-ma/>.
- [94] E. Riensche, J. Meusinger, U. Stimming, G. Unverzag, Optimization of a 200 kW SOFC cogeneration power plant. Part II: Variation of the flowsheet, *J. Power Sources*. 71 (1998) 306-314.
- [95] R.-U. Dietrich, J. Oelze, A. Lindermeir, C. Spitta, M. Steffen, T. Küster, S. Chen, C. Schlitzberger, R. Leithner, Efficiency gain of solid oxide fuel cell systems by using anode offgas recycle - Results for a small scale propane driven unit, *J. Power Sources*. 196 (2011) 7152-7160.
- [96] M. Noponen, M. Halinen, J. Saarinen, J. Kiviaho, Experimental study of anode gas recycling on efficiency of SOFC, *ECS Transactions*. 5 (2007) 545-551.
- [97] D. Larrain, J. Van herle, D. Favrat, Simulation of SOFC stack and repeat elements including interconnect degradation and anode reoxidation risk, *J. Power Sources*. 161 (2006) 392-403.
- [98] M.P. Heddrich, M. Jahn, A. Michaelis, R. Näge, A. Weder, SOFC system design using ideal efficiency modeling - Model and experimental implementation, *Fuel Cells*. 13 (2013) 612-622.
- [99] R. Peters, E. Riensche, P. Cremer, Pre-reforming of natural gas in solid oxide fuel-cell systems, *J. Power Sources*. 86 (2000) 432-441.
- [100] A. Nummela, M. Noponen, Experimental Study on Effects of Anode Recirculation to Pre-Reforming of Natural Gas, *European Fuel Cell Forum*. B0301 (2009).

- [101] D.G. Goodwin, An open-source, extensible software suite for CVD process simulation, In Proceedings of CVD XVI and EuroCVD 14, M. Allendorf, F. Maury, and E. Teyssandier, Eds, PV 2003-2008.
- [102] G.P. Smith, GRI-MECH 3.0, 2009, Last accessed 03.04 2015, <http://combustion.berkeley.edu/gri-mech/>.
- [103] A. Selimovic, M. Kemm, T. Torisson, M. Assadi, Steady state and transient thermal stress analysis in planar solid oxide fuel cells, J. Power Sources. 145 (2005) 463-469.
- [104] M. Pihlatie, T. Ramos, A. Kaiser, Testing and improving the redox stability of Ni-based solid oxide fuel cells, J. Power Sources. 193 (2009) 322-330.
- [105] A. Wood, M. Pastula, D. Waldbilig, D.G. Ivey, Initial testing of solutions to redox problems with anode-supported SOFC, J. Electrochem. Soc. 153 (2006) A1929-A1934.
- [106] Q. Jeangros, A. Faes, J.B. Wagner, T.W. Hansen, U. Aschauer, J. Van herle, A. Hessler-Wyser, R.E. Dunin-Borkowski, In situ redox cycle of a nickel-YSZ fuel cell anode in an environmental transmission electron microscope, Acta Materialia. 58 (2010) 4578-4589.
- [107] M. Pihlatie, A. Kaiser, M. Mogensen, Redox stability of SOFC: Thermal analysis of Ni-YSZ composites, Solid State Ionics. 180 (2009) 1100-1112.
- [108] J.F.B. Rasmussen, P.V. Hendriksen, A. Hagen, Study of internal and external leaks in tests of anode-supported SOFCs, Fuel Cells. 8 (2008) 385-393.
- [109] R. Peters, R. Deja, L. Blum, J. Pennanen, J. Kiviaho, T. Hakala, Analysis of solid oxide fuel cell system concepts with anode recycling, Int J Hydrogen Energy. 38 (2013) 6809-6820.
- [110] Guidechem.com, Nickel carbonyl(Ni(CO)₄), (cas 13463-39-3) msds, 2014, Last accessed 11/21 2014, <http://www.guidechem.com/msds/13463-39-3.html>.
- [111] Matheson Tri Gas, Material safety data sheet nickel carbonyl, 2008, Last accessed 03.04 2015, <https://www.mathesongas.com/pdfs/msds/MAT16290.pdf>.
- [112] L. Petruzzi, S. Cocchi, F. Fineschi, A global thermo-electrochemical model for SOFC systems design and engineering, J. Power Sources. 118 (2003) 96-107.
- [113] H. Apfel, M. Rzepka, H. Tu, U. Stimming, Thermal start-up behaviour and thermal management of SOFC's, J. Power Sources. 154 (2006) 370-378.
- [114] D.L. Damm, A.G. Fedorov, Reduced-order transient thermal modeling for SOFC heating and cooling, J. Power Sources. 159 (2006) 956-967.

- [115] B. Borglum, E. Tang, M. Pastula, Development of solid oxide fuel cells at versa power systems, ECS Transactions. 35 (2011) 63-69.
- [116] Y.-S. Chou, J.W. Stevenson, Compressive mica seals for solid oxide fuel cells, ASM Conference Proceedings: Joining of Advanced and Specialty Materials. (2005) 132-139.
- [117] M. Bram, S. Reckers, P. Drinovac, J. Mönch, R.W. Steinbrech, H.P. Buchkremer, D. Stöver, Deformation behavior and leakage tests of alternate sealing materials for SOFC stacks, J. Power Sources. 138 (2004) 111-119.
- [118] Y.-S. Chou, J.W. Stevenson, L.A. Chick, Ultra-low leak rate of hybrid compressive mica seals for solid oxide fuel cells, J. Power Sources. 112 (2002) 130-136.
- [119] Y.-S. Chou, J.W. Stevenson, L.A. Chick, Novel compressive mica seals with metallic interlayers for solid oxide fuel cell applications, J Am Ceram Soc. 86 (2003) 1003-1007.
- [120] Y. Chou, J.W. Stevenson, Long-term ageing and materials degradation of hybrid mica compressive seals for solid oxide fuel cells, J. Power Sources. 191 (2009) 384-389.
- [121] Y.-S. Chou, J.W. Stevenson, Infiltrated phlogopite micas with superior thermal cycle stability as compressive seals for solid oxide fuel cells, Ceramic Transactions. 161 (2005) 89-98.
- [122] Y.-S. Chou, J.W. Stevenson, J. Hardy, P. Singh, Material degradation during isothermal ageing and thermal cycling of hybrid mica seals under solid oxide fuel cell exposure conditions, J. Power Sources. 157 (2006) 260-270.
- [123] Y.-S. Chou, J.W. Stevenson, Novel infiltrated Phlogopite mica compressive seals for solid oxide fuel cells, J. Power Sources. 135 (2004) 72-78.
- [124] Y.-S. Chou, J.W. Stevenson, P. Singh, Thermal cycle stability of a novel glass-mica composite seal for solid oxide fuel cells: Effect of glass volume fraction and stresses, J. Power Sources. 152 (2005) 168-174.
- [125] P. Batfalsky, V.A.C. Haanappel, J. Malzbender, N.H. Menzler, V. Shemet, I.C. Vinke, R.W. Steinbrech, Chemical interaction between glass-ceramic sealants and interconnect steels in SOFC stacks, J. Power Sources. 155 (2006) 128-137.
- [126] F. Wiener, M. Bram, H.-P. Buchkremer, D. Sebold, Chemical interaction between Crofer 22 APU and mica-based gaskets under simulated SOFC conditions, J. Mater. Sci. 42 (2007) 2643-2651.

- [127] M. Bram, L. Niewolak, N. Shah, D. Sebold, H.P. Buchkremer, Interaction of sealing material mica with interconnect steel for solid oxide fuel cells application at 600 °C, *J. Power Sources*. 196 (2011) 5889-5896.
- [128] Y.-S. Chou, J.W. Stevenson, J.-P. Choi, Long-term evaluation of solid oxide fuel cell candidate materials in a 3-cell generic short stack fixture, Part II: Sealing glass stability, microstructure and interfacial reactions, *J. Power Sources*. 250 (2014) 166-173.
- [129] J.R. Hoyes, S. Bond, Gaskets for sealing solid oxide fuel cells, *Sealing Technology*. (2007) 11-14.
- [130] D. Goedeke, J. Besinger, Y. Pflügler, B. Ruedinger, New Glass Ceramic Sealants for SOFC, *ECS Transactions*. 25 (2009) 1483-1490.
- [131] Y.-S. Chou, J.W. Stevenson, Novel infiltrated Phlogopite mica compressive seals for solid oxide fuel cells, *J. Power Sources*. 135 (2004) 72-78.
- [132] J.G. Grolig, J. Froitzheim, J.-E. Svensson, Coated stainless steel 441 as interconnect material for solid oxide fuel cells: Oxidation performance and chromium evaporation, *J. Power Sources*. 248 (2014) 1007-1013.
- [133] J.R. Hoyes, M. Rautanen, SOFC sealing with thermiculite 866 and thermiculite 866 LS, *ECS Transactions*. 57 (2013) 2365-2374.
- [134] M.W. Lundberg, R. Berger, J. Westlinder, N. Folkesson, H. Holmberg, Novel multilayered PVD-coating in a roll to roll mass production process, *ECS Transactions*. 57 (2013) 2203-2208.
- [135] K. Lee, J. Yun, K. Ahn, S. Lee, S. Kang, S. Yu, Operational characteristics of a planar steam reformer thermally coupled with a catalytic burner, *Int J Hydrogen Energy*. 38 (2013) 4767-4775.
- [136] A. Pohjoranta, M. Halinen, J. Pennanen, J. Kiviaho, Solid oxide fuel cell stack temperature estimation with data-based modeling - Designed experiments and parameter identification, *J. Power Sources*. 277 (2015) 464-473.

Title	Improved durability and reduced system complexity of solid oxide fuel cell systems
Author(s)	Olivier Thomann
Abstract	<p>Solid oxide fuel cells (SOFCs) show great potential for clean and efficient power generation applications. However, their high cost is preventing their market entry. This dissertation focuses on solutions to increase the durability of SOFCs and to reduce the complexity of SOFC systems to drive their cost down.</p> <p>Chromium poisoning of the cathode is a major issue limiting the durability of SOFCs. This issue is addressed by the development of a protective manganese-cobalt spinel coating for steel interconnects. Coated interconnects were characterised in SOFC relevant conditions and the results showed that the coating fulfilled its main requirements, which are: limitation of chromium transport from the interconnect to the cathode, protection against oxidation of the steel and low and stable area-specific resistance. Evidence was found that another source of chromium is the balance-of-plant (BoP) components upstream of the cathode, an issue which did not receive much attention in the literature. Therefore, a method for measuring chromium evaporation from BoP components was developed and validated on a stainless steel pipe.</p> <p>SOFC systems based on natural gas commonly include a fuel processing subsystem for fuel steam reforming. The need for an external water source can be eliminated by recycling the steam-rich anode off-gas. Investigations were performed on a pre-reformer with a precious metal catalyst and it was found that adding an anode off-gas recycling loop had no detrimental effect on the activity of the catalyst and carbon formation could be avoided. Additionally, results showed the possibility to generate the hydrogen-containing gas needed to prevent the reoxidation of the anode catalyst during heat-up phase. The results permitted the implementation of an anode off-gas recycling loop in a 10 kW SOFC system.</p> <p>Additionally, the system was heated up without supplying any premixed hydrogen-containing gas, which enables to reduce the complexity of the system.</p> <p>Finally, the durability of a stack can be improved by seal solutions with limited material interactions. A hybrid seal solution was developed by coating a compressible core with glass layers. The developed seal reduced the leak rate compared to a purely compressible seal. Material interactions were studied with a post-experimental investigation of an SOFC stack. Interactions were limited with the exception of evidence of increased oxidation at the steel/seal/air interface.</p> <p>Overall, the solution was found to be promising and the obtained results led to the commercialisation of the developed seal solution by Flexitallic Ltd (UK).</p>
ISBN, ISSN, URN	<p>ISBN 978-951-38-8360-7 (Soft back ed.)</p> <p>ISBN 978-951-38-8361-4 (URL: http://www.vttresearch.com/impact/publications)</p> <p>ISSN-L 2242-119X</p> <p>ISSN 2242-119X (Print)</p> <p>ISSN 2242-1203 (Online)</p> <p>http://urn.fi/URN:ISBN:978-951-38-8361-4</p>
Date	December 2015
Language	English
Pages	85 p. + app. 57 p.
Name of the project	
Commissioned by	
Keywords	Fuel cells, SOFC, chromium poisoning, anode off-gas recycling, system heat-up, seal, interconnect, material interactions
Publisher	VTT Technical Research Centre of Finland Ltd P.O. Box 1000, FI-02044 VTT, Finland, Tel. 020 722 111

Improved durability and reduced system complexity of solid oxide fuel cell systems

Solid oxide fuel cells (SOFCs) are electrochemical devices that produce electricity (and heat) from fuel and air. They are expected to play an important role in the power generation sector due to their advantages in terms of high electrical efficiency, modularity, fuel flexibility and very low emissions. However, their high cost remains a burden, delaying their market entry. In order to drive their cost down, their durability must be improved and the system complexity needs to be reduced. This dissertation addresses these challenges through the development of solutions to reduce the degradation of SOFCs because of chromium poisoning of the cathode. In addition, simplification of the fuel processing subsystem are investigated and demonstrated. Lastly, performant and durable sealing solutions were developed and tested in an operating SOFC stack.

ISBN 978-951-38-8360-7 (Soft back ed.)
ISBN 978-951-38-8361-4 (URL: <http://www.vttresearch.com/impact/publications>)
ISSN-L 2242-119X
ISSN 2242-119X (Print)
ISSN 2242-1203 (Online)
<http://urn.fi/URN:ISBN:978-951-38-8361-4>

